Engineering Structures 300 (2024) 117173

Contents lists available at ScienceDirect

Engineering Structures

journal homepage: www.elsevier.com/locate/engstruct

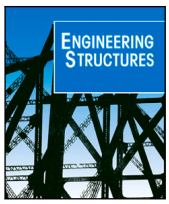

Stress projection procedure for the form-finding analysis of membrane structures

Rostislav Lang [a,b,*], Ivan Němec [a,b], K.C. Park [c]

[a] Brno University of Technology, Faculty of Civil Engineering, Institute of Structural Mechanics, Veveří 331/95, 602 00 Brno, Czech Republic
[b] FEM consulting, s.r.o.Veveří 331/95, 602 00 Brno, Czech Republic
[c] Ann and H. J. Smead Aerospace Engineering Sciences, University of Colorado, Boulder, CO 80309-429, USA

ARTICLE INFO

Keywords:
Form-finding
Force-finding
Equilibrium searching
Stress projection
Stress density
Distortion control
Element size control
Stress adaptation
Membrane structure
Shell structure optimization

ABSTRACT

This study examines the form-finding analysis of membrane structures and presents a new general method for determining prestress called stress projection. This method addresses several deficiencies while performing the form-finding analysis, especially in the case of conical membrane structures. A key feature of the proposed stress projection procedure is the adoption of a generally oriented projection plane, where finite elements are projected onto, and the determination of their stress states, which allows for a smooth adaptation of stresses over the membrane structures. Deformation gradients are then evaluated with respect to this projection plane, as opposed to the inertial reference frame used for the computation of stress tensors in subsequent form-finding processes.

The proposed stress projection procedure efficiently modifies the stresses over the structures and significantly addresses intrinsic element distortion problems within the form-finding analysis. Thus, the proposed method allows for the maintenance of regularized finite element shapes and the smooth changing of stress states throughout form-finding iteration processes, especially for conical membrane shapes. Numerical experiments demonstrate the efficiency of the implemented stress projection scheme compared with two well-known stress adaptation schemes.

1. Introduction

The design process of membrane structures is inherently connected to a form-finding analysis that aims to identify the equilibrium shape based on the required prestress, loading, and boundary conditions. The shapes of such structures are related to the equilibrium of tensile forces in space. In addition to searching for the initial equilibrium positions of membrane and cable structures, form-finding analysis can be utilized to optimize the shapes of shell and girder structures subjected to a given load.

The term "form-finding" emphasizes the search for final shapes. However, this is not the only task involved, as equilibrium states are generally unknown in advance. The form-finding analysis thus searches for both the shape and the equilibrium state derived from the required prestress values. As mentioned in many studies, the only prestress that can be prescribed in advance and is consequently reached is isotropic prestress, if the equilibrium shape can physically exist, as will be discussed later. Furthermore, as proven in a number of studies, constant anisotropic prestress is not a viable choice to reach the equilibrium shape within form-finding analysis.

As a consequence of the above, the prestress, defined as a form-finding input, must be adapted to reach the equilibrium shape. Without a stress adaptation procedure, the form-finding procedure will not succeed. According to Linhard et al. [1], "It is possible to stabilize the form finding process with the proposed stress adaptation scheme". Following this, the terms "stress adaptation", "stress adaptation scheme", and "stress adaptation procedure" are utilized in this study. The aim of this work is to introduce a new stress adaptation scheme called stress projection and to present its benefits for conical membrane structures.

1.1. Motivation

Before the proposed stress projection scheme is described, well-known stress adaptation schemes are reviewed. The most common ones involve force density and stress density [2–6], hence the names force density method (FDM) and stress density method (SDM). These adaptations are based on push-forward operations between the original and equilibrium configurations, as will be described later in this paper. Furthermore, distortion control and element size control [1,7–10] procedures are reviewed.

* Corresponding author at: Brno University of Technology, Faculty of Civil Engineering, Institute of Structural Mechanics, Veveří 331/95, 602 00 Brno, Czech Republic.
E-mail addresses: lang.r@fce.vutbr.cz (R. Lang), nemec.i@fce.vutbr.cz (I. Němec), kcpark@colorado.edu (K.C. Park).

https://doi.org/10.1016/j.engstruct.2023.117173
Received 26 June 2023; Received in revised form 12 October 2023; Accepted 12 November 2023
Available online 20 November 2023

A critical review of existing stress adaptation procedures identifies the sources of an undesirable interconnection between the final equilibrium shape and the initial position of the structure while performing form-finding analysis. This unwanted interconnection, which is characteristic of current stress adaptations, often leads to a compromise between the required configuration and the final equilibrium state. The proposed stress projection procedure efficiently prevents such a deficiency, which makes this method unique compared to other stress adaptation schemes.

The stress projection scheme removes the undesired dependency by introducing a generally oriented projection plane. On this plane, all elements are projected to determine their fictitious deformation gradients and, subsequently, the stress state within the structure. The equilibrium stress field in the projection plane is determined analytically, as presented in the derived formula. This stress field is further utilized for the mapping process to determine the equilibrium stress within the structure. The analytically determined stress field in the projection plane is the first of the true sources of the discrepancy removal mentioned above. The projection of particular finite elements onto the projection plane generally changes, as will be presented later on, and is the second true source of discrepancy removal. The objective of the proposed stress projection procedure is to provide the possibility of reaching smoothly changing and well-distributed prestress in conical membrane structures.

From a finite element formulation perspective, the stress states utilized in the proposed stress projection procedure may be viewed as the regularized element shapes used. This is because the projected element shapes yield the intermediate strain states between both extreme configurations, that is, the total Lagrangian strain states and the Eulerian strain states. In fact, the adoption of a common projection plane is shown to eliminate the undesirable dependency between the final equilibrium shape and the initial shape or the mesh discretization used. The numerical experiments presented here confirm the desirable properties of the proposed stress projection procedure.

1.2. Review of existing form-finding methods

Many form-finding methods have been proposed to date. Linkwitz and Schek's [2,3] well-known FDM was derived from the nodal equilibrium conditions for cable net structures. In its basic form, the method linearizes the form-finding analysis. This is achieved by using the assumption of a proportional relationship between the force and the length of a cable, the so-called force density, which accounts for the name of the form-finding method.

Haber and Abel proposed the assumed geometric stiffness method (AGSM) [4,11], which is consistently derived from the linearized form of the virtual work equation. In addition to cable net structures, this method is applicable to membranes and other types of structures. It assumes that form-finding analysis is basically independent of the material used. Therefore, the material part of the linearized equation of virtual work is completely removed from the process, leaving only the part connected with the work of the nonlinear part of the Green–Lagrange strain tensor increment. With the use of the standard formula for the geometric stiffness matrix, the proportionality between the force and the length, or the stress and the size, is incorporated, and the resulting stress state can be calculated as a push-forward operation of the initially prescribed prestress values. Therefore, the AGSM can be perceived as a consistent generalization of the FDM.

The assumption of proportionality between the prestress and the size is a strict stress adaptation scheme within form-finding analysis. Managing the process of reaching the desirable smooth and rather uniform prestress in a membrane structure is difficult using this precondition. As described in the aforementioned articles, both FDM and AGSM can be used in a nonlinear manner if the stress state is not obtained by the push-forward operation between the initial and actual configurations. However, this principally removes the essential stress adaptation from the form-finding analysis, which must be replaced with another one.

The updated reference strategy (URS) proposed by Bletzinger and Ramm [12] is a form-finding method that incorporates the mixed formulation of the reference and the actual configurations. As in the case of the FDM and AGSM, the URS also assumes the essential form-finding analysis independence of the material used. The stress adaptation procedures covered most frequently within the URS by Bletzinger et al. [1,7,8] are distortion control and element size control. These techniques use a stress-to-size ratio when a particular finite element exceeds the allowed deformation without affecting the stress up to this limit. Another stress adaptation scheme presented by Bletzinger et al. [7,13] is the assumption of a relation between the prestress in the final configuration of a membrane structure and the stress defined in the related configuration, the so-called reference strip, which refers to the production process of these structures. The force incompatibilities in the positions of the common lines of the adjacent reference strips are suggested to be avoided using distortion control or element size control.

Tabarrok and Qin [14] proposed a classical form of the linearized equation of virtual work to be used for form-finding analysis. The stress adaptation incorporated is based on the assumption of a very small Young's modulus. By including this fictitious material, the prescribed unrealizable prestress is modified to reach the final equilibrium in a standard way of structural analysis.

Barnes [15,16] proposed the use of dynamic relaxation (DR) within form-finding analysis. An overview of various form-finding methods, including their comparison, was presented by Veenendaal and Block [17] and Tibert and Pellegrino [18] for tensegrity structures. Further related literature by various authors can be found in [19–29].

1.3. Basic features of form-finding analysis

In theory, form-finding analysis is independent of both the material used and the initial shape of the structure, provided it is possible to predefine the equilibrium. In principle, the final shape depends exclusively on the equilibrium of forces within the given boundary conditions. However, predefining equilibrium prestress in advance is generally impossible [4,19] except of a unique situation when using isotropic prestress. Nevertheless, if the isotropic prestress does not meet the engineering requirements for the structure, or if it cannot even physically exist, as shown in Fig. 2, the use of general anisotropic prestress is necessary. Using constant anisotropic prestress for double-curved surfaces is not physically possible, as shown in Fig. 1. In fact, the essential need to search for general anisotropic prestress in equilibrium is the real reason why various stress adaptation schemes have been formulated within form-finding analysis. General anisotropic prestress is usually derived from a defined simple prestress input, which is only given by two values: one in the warp direction and in the weft direction. Thus, the stress adaptation procedures lead to the general anisotropic prestress in equilibrium within a membrane structure and modify the initially physically incompatible input values.

It is important to emphasize the idea above that the resulting prestress distribution obtained within the form-finding analysis is principally independent of the material. This is the consequence of the essential fact that stress in a structure is not a response to deformation, as in the case of a standard structural analysis. On the other hand, the specified prestress is the basic shaping parameter of form-finding analysis, as described extensively by Bletzinger et al. [1,7–9,12,13].

The demonstrative example below shows the utilization of constant anisotropy in form-finding analysis, which is strictly required. However, the corresponding equilibrium configuration with this requirement cannot exist for a double-curved surface, as such a prestress is in equilibrium for zero Gaussian curvature [1,19] only. Therefore, such an input of form-finding analysis leads to a diverging process, as shown in Fig. 1.

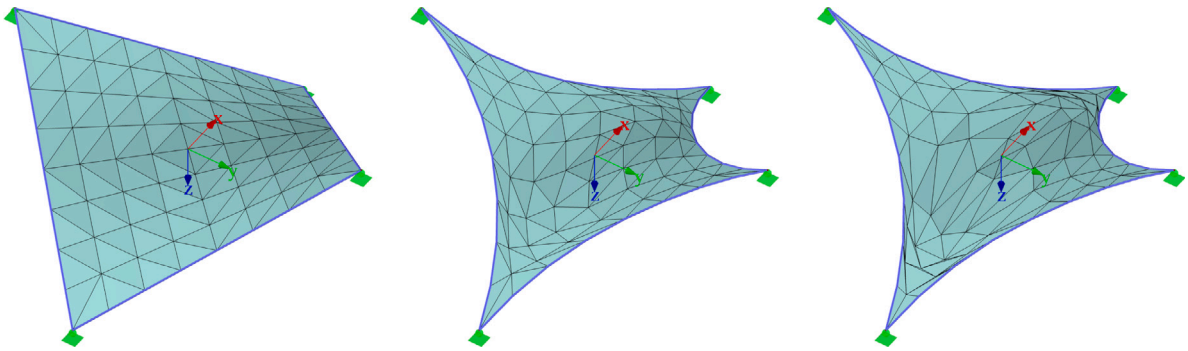

Fig. 1. Initial configuration (left) and diverging form-finding analysis for constant anisotropy (middle, right).

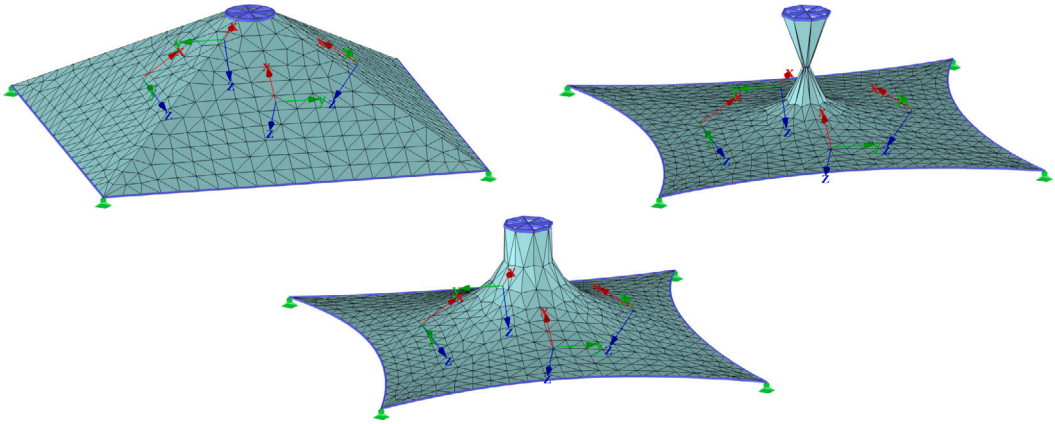

Fig. 2. Initial configuration (left) and collapsing shape utilizing isotropy prestress (middle, right).

As mentioned above, the only equilibrium state that is possible to predefine in advance is isotropic prestress. However, the feasibility of such a prestress can be violated by external loading or the given boundary conditions, which do not allow such a prestress to exist. A typical example is conical membrane structures, which have a tendency toward necking and collapsing. By using the isotropic prestress for these membrane structures, the equilibrium configuration cannot usually be physically reached, as proven by the collapsing shape in Fig. 2. This collapse susceptibility is related to the proportion between the height and the bases of the conical membrane structure, which is called the critical height [19,30]. The structure collapses after exceeding this critical height.

As most conical membrane structures are susceptible to collapse, they require a general anisotropic prestress. As mentioned above, such a prestress is practically impossible to predefine, which is why stress adaptation schemes are needed to solve this situation and reach the required equilibrium. The need for equilibrium searching is virtually the main objective problem in form-finding analysis. This identifies the essential requirements of stress adaptation schemes within form-finding analysis, which are responsible for reaching equilibrium.

As already mentioned, different methods have been proposed, as summarized in [17], which can be used to adapt stresses and thus reach the equilibrium. The well-known force density [2,3,17] and stress density [4], however, are highly strict stress adaptations when used in their linear forms. They often lead to overstressed areas. Distortion control and element size control [1,7–9] assume stress adaptations after exceeding a predefined deformation or allowable configuration. Although these techniques decrease the stress peaks, they also bring an on–off switch into stress adaptation. They also lead to unnecessary in-plane deformations of elements to start the needed stress adaptation. By using reference strips as reference configurations for stress definition, incompatibility problems may arise in the areas of the common seam lines of a membrane structure [7,13]. Thus, combining methods is necessary. Another possible option is the incorporation of a fictitious soft material [14], but this also causes overstressed areas in some parts. All these methods exhibit dependency on FE mesh discretization or on the original shape when the equilibrium is to be searched. Alternatively, interaction with such methods is needed when using reference strips. Controlling the stress adaptations in different parts of conical membrane structures is also difficult to reach smoothly distributed prestress. For this reason, stress projection is proposed, which is especially suitable for conical membrane structures. This stress adaptation technique is independent of both FE mesh discretization and the initial position of the structure, which is a unique quality of stress adaptation schemes.

2. Formulation of form-finding analysis

Regarding the later utilization of stress adaptation procedures, the applied implicit form-finding method is described first. Two well-known stress adaptation procedures are described later. The stress projection procedure is also described in detail, followed by a comparison given in tabular form. Continuum mechanics equations are mentioned for the purpose of the form-finding method used.

2.1. Continuum mechanics equations

The governing equation of the virtual work variation of internal forces δW^{int} and external forces δW^{ext} is recalled below (1). The parts are expressed in terms of the actual structure configurations. This corresponds to the updated Lagrangian formulation, which was utilized during the implementation of the form-finding analysis that will be described later on. It is important to note that the total Lagrangian formulation or the utilization of the explicit formulation via

DR would not change the physical meaning of the proposed stress projection procedure. The proposed stress projection described later is exclusively a stress adaptation procedure that is fully compatible with any formulation mentioned here. Thus, the only reason for reviewing the updated Lagrangian formulation is that this method was utilized during the implementation work of the presented method.

$$\int_{{}^{i}V} {}^{i+1}\mathbf{S}\delta^{i+1}\mathbf{E}\, dV = \int_{{}^{i}V} {}^{i+1}\mathbf{f}\delta^{i+1}\mathbf{u}\, dV, \tag{1}$$

where i and $i+1$ are the calculation step last performed and the calculation step to be solved, respectively; ${}^{i}V$ is the actual configuration of the structure, obtained in calculation step i; ${}^{i+1}\mathbf{S}$ is the second Piola–Kirchhoff strain tensor; $\delta^{i+1}\mathbf{E}$ is the Green–Lagrange strain tensor variation in step $i+1$ to be solved; ${}^{i+1}\mathbf{f}$ is the generalized forces in step $i+1$, expressed in terms of the actual configuration ${}^{i}V$; and $\delta^{i+1}\mathbf{u}$ is the deformation variations.

The second Piola–Kirchhoff stress ${}^{i+1}\mathbf{S}$ and the Green–Lagrange strain ${}^{i+1}\mathbf{E}$ tensors are decomposed below. The already known expressions ${}^{i}\mathbf{S}$ and ${}^{i}\mathbf{E}$, describing the state in the actual configuration in step i and the expressions for the unknown states of the structures $\Delta\mathbf{S}$ and $\Delta\mathbf{E}$, are separated. Note that the stress state in step i, described by the second Piola–Kirchhoff stress tensor ${}^{i}\mathbf{S}$, expressed in terms of the actual configuration ${}^{i}V$, corresponds to the Cauchy stress tensor $\boldsymbol{\sigma}$, so ${}^{i}\mathbf{S} = \boldsymbol{\sigma}$. Furthermore, when decomposing the Green–Lagrange strain tensor ${}^{i+1}\mathbf{E}$ into parts ${}^{i}\mathbf{E}$ and $\Delta\mathbf{E}$, the strain tensor increment is related to the actual configuration ${}^{i}\mathbf{E} = 0$. Thus, the following equations result:

$${}^{i+1}\mathbf{S} = {}^{i}\mathbf{S} + \Delta\mathbf{S} = \boldsymbol{\sigma} + \Delta\mathbf{S}, \qquad {}^{i+1}\mathbf{E} = {}^{i}\mathbf{E} + \Delta\mathbf{E} = \Delta\mathbf{E} = \Delta\boldsymbol{\epsilon} + \Delta\boldsymbol{\eta}, \tag{2}$$

where $\Delta\boldsymbol{\epsilon}$ and $\Delta\boldsymbol{\eta}$ correspond to the linear and nonlinear parts of the Green–Lagrange strain tensor increment $\Delta\mathbf{E}$, respectively.

When using the expressions of (2) within Eq. (1), the expression of the virtual work variations written out in parts is obtained.

$$\int_{{}^{i}V} \Delta\mathbf{S}\delta\Delta\boldsymbol{\epsilon}\, dV + \int_{{}^{i}V} \Delta\mathbf{S}\delta\Delta\boldsymbol{\eta}\, dV + \int_{{}^{i}V} \boldsymbol{\sigma}\delta\Delta\boldsymbol{\epsilon}\, dV + \int_{{}^{i}V} \boldsymbol{\sigma}\delta\Delta\boldsymbol{\eta}\, dV = \int_{{}^{i}V} {}^{i+1}\mathbf{f}\delta^{i+1}\mathbf{u}\, dV. \tag{3}$$

By modifying the increment of the second Piola–Kirchhoff stress tensor $\Delta\mathbf{S}$ with the Taylor series and after assuming linear approximation, we obtain the following:

$$\Delta\mathbf{S} = \frac{\partial^{i}\mathbf{S}}{\partial^{i}\mathbf{E}}\Delta\mathbf{E} + \cdots \doteq \frac{\partial^{i}\mathbf{S}}{\partial^{i}\mathbf{E}}(\Delta\boldsymbol{\epsilon} + \Delta\boldsymbol{\eta}) \doteq \mathbf{C}\Delta\boldsymbol{\epsilon}, \tag{4}$$

where $\mathbf{C}$ denotes the constitutive material law. After substituting (4) into the first term of (3) and neglecting its second term, and then multiplying the second Piola–Kirchhoff stress tensor increment $\Delta\mathbf{S}$ to the nonlinear part of the Green–Lagrange strain tensor increment $\Delta\boldsymbol{\eta}$, we obtain the general linearized equation of virtual work, which is the essential basis of the form-finding method described in the following chapter.

$$\int_{{}^{i}V} \mathbf{C}\Delta\boldsymbol{\epsilon}\delta\Delta\boldsymbol{\epsilon}\, dV + \int_{{}^{i}V} \boldsymbol{\sigma}\delta\Delta\boldsymbol{\eta}\, dV = \int_{{}^{i}V} {}^{i+1}\mathbf{f}\delta^{i+1}\mathbf{u}\, dV - \int_{{}^{i}V} \boldsymbol{\sigma}\delta\Delta\boldsymbol{\epsilon}\, dV. \tag{5}$$

Utilizing finite elements (FE) discretization, the strain components $\Delta\boldsymbol{\epsilon}$ and $\Delta\boldsymbol{\eta}$, corresponding to the linear and nonlinear parts of the Green–Lagrange strain tensor, can be expressed as

$$\Delta\boldsymbol{\epsilon} = \mathbf{B}_{Lk}\Delta\mathbf{u}_k, \qquad \Delta\boldsymbol{\eta} = \mathbf{B}_{NLk}\Delta\mathbf{u}_k, \tag{6}$$

where $\mathbf{B}_{Lk}$ and $\mathbf{B}_{NLk}$ are the linear and nonlinear strain interpolation matrices, respectively, which are each assembled for the actual configurations. After assuming discretization and substituting (6) into (5), as well as removing the displacement variations, the linearized equation of the virtual work variations appears in the following discretized form:

$$\sum_{k}^{m} \int_{{}^{i}V_k} \mathbf{B}_{Lk}^{T}\mathbf{C}_k\mathbf{B}_{Lk}\, dV_k\Delta\mathbf{u}_k + \sum_{k}^{m} \int_{{}^{i}V_k} \mathbf{B}_{NLk}^{T}\boldsymbol{\sigma}_k\mathbf{B}_{NLk}\, dV_k\Delta\mathbf{u}_k = \sum_{k}^{m} \int_{{}^{i}V_k} {}^{i+1}\mathbf{f}_k\, dV_k - \sum_{k}^{m} \int_{{}^{i}V_k} \mathbf{B}_{Lk}^{T}\vec{\boldsymbol{\sigma}}_k\, dV_k, \tag{7}$$

where k and m denote the currently considered finite element and the total number of finite elements, respectively, and $\Delta\mathbf{u}_k$ represents a vector of the discretized displacement increments.

Expressed in the matrix form, the material stiffness matrix $\mathbf{K}_{Lk}$ and the geometrical stiffness matrix $\mathbf{K}_{NLk}$, as well as the vectors of the external nodal forces ${}^{i+1}\mathbf{F}_k^{ext}$ and the internal nodal forces ${}^{i}\mathbf{F}_k^{int}$, are obtained, and Eq. (7) can be written in the following form:

$$\sum_{k}^{m} \mathbf{K}_{Lk}\Delta\mathbf{u}_k + \sum_{k}^{m} \mathbf{K}_{NLk}\Delta\mathbf{u}_k = \sum_{k}^{m} {}^{i+1}\mathbf{F}_k^{ext} - \sum_{k}^{m} {}^{i}\mathbf{F}_k^{int}. \tag{8}$$

The governing equations of the equilibrium for solving the nonlinear analysis are recalled in the continuum and the discretized form here. These equations are the bases for the general form-finding method described in the following section.

2.2. Form-finding method

The form-finding method utilized for the subsequent presentation of stress adaptation techniques is derived from the general equation of equilibrium described above. As the stress adaptation schemes presented in this study are mapping based and thus principally material independent, the increment of the linear part of the Green–Lagrange strain tensor $\Delta\boldsymbol{\epsilon}$ does not influence the equilibrium at all. This corresponds with the assumptions of Haber and Abel [4] and with the categorization between geometric stiffness methods according to Veenendaal and Block [17]. Therefore, the following reduced forms of Eqs. (5), (7), and (8) can be used in the form-finding analysis:

$$\int_{{}^{i}V} \boldsymbol{\sigma}\delta\Delta\boldsymbol{\eta}\, dV = \int_{{}^{i}V} {}^{i+1}\mathbf{f}\delta^{i+1}\mathbf{u}\, dV - \int_{{}^{i}V} {}^{i}\boldsymbol{\sigma}\delta\Delta\boldsymbol{\epsilon}\, dV, \tag{9}$$

$$\sum_{k}^{m} \int_{{}^{i}V_k} \mathbf{B}_{NLk}^{T}\boldsymbol{\sigma}_k\mathbf{B}_{NLk}\, dV_k\Delta\mathbf{u}_k = \sum_{k}^{m} \int_{{}^{i}V_k} {}^{i+1}\mathbf{f}_k\, dV_k - \sum_{k}^{m} \int_{{}^{i}V_k} \mathbf{B}_{Lk}^{T}\vec{\boldsymbol{\sigma}}_k\, dV_k, \tag{10}$$

$$\sum_{k}^{m} \mathbf{K}_{NLk}\Delta\mathbf{u}_k = \sum_{k}^{m} {}^{i+1}\mathbf{F}_k^{ext} - \sum_{k}^{m} {}^{i}\mathbf{F}_k^{int}. \tag{11}$$

The reduced equations are the convenient bases for a numerical solution for the form-finding analysis. However, it is important to emphasize that the stress projection procedure that will be presented later is not restricted to a particular form-finding method, but can be utilized within any of the general methods mentioned in the introduction without any problem. Generally, as already indicated above, stress adaptation schemes are required to reach the equilibrium. Such methods will be discussed later in this paper.

2.3. Mapping-based stress adaptation procedures

It must be emphasized that the applied stress adaptation procedure is completely responsible for reaching the final equilibrium shape. The resulting stress state is always artificial in principle because it is not a response of the structure but a driving parameter of the form-finding process. The objective task of the form-finding analysis is to reach the equilibrium, while it is most desirable to have the resulting stresses well distributed, thus smoothly changing and without any concentrations, if physically possible.

Several well-known stress adaptation procedures have been mentioned in the introduction. Two of them, stress density and distortion control, are described in detail below. Both methods are principally material independent and are also widely used within form-finding analysis. This description will be used later for a comparison with the proposed stress projection. The comparison provides a deeper understanding of and insight into the new method.

2.3.1. Stress density

Under the presumption of a consistent linearization of form-finding analysis, the resulting stress state is obtained using the push-forward operation. This mapping process between the initial and actual configurations introduces stress changes that are dependent on changes in the finite element shape. Inspired by the nomenclature of force density proposed by Linkwitz and Schek [2,3], the generalized concept for an arbitrary finite element is called stress density.

Let us assume that the prestress is defined with respect to the initial configuration of the structure, that is, in the step $i = 0$. Thus, the second Piola–Kirchhoff stress tensor ${}^0\mathbf{S}$ is prescribed as a form-finding input.

When assembling Eqs. (9)–(11) for the first form-finding step $i = 1$, the Cauchy stress tensor ${}^0\boldsymbol{\sigma}$ related to configuration ${}^0V_k$ corresponds with the second Piola–Kirchhoff stress tensor, as both refer to the same initial configuration. Thus, using the expression ${}^0\boldsymbol{\sigma} = {}^0\mathbf{S}$ for the procedure described by Eqs. (9)–(11) is possible to obtain a new configuration in step $i = 1$. As there is no material constitutive law included, the second Piola–Kirchhoff stress tensor increment is zero $\Delta\mathbf{S}$, and it can be written as ${}^i\mathbf{S} = {}^0\mathbf{S}$. As the second Piola–Kirchhoff stress tensor ${}^i\mathbf{S}$ is known, it can be used further for stress estimation within the actual configuration ${}^iV_k$. Therefore, the Cauchy stress tensor ${}^i\boldsymbol{\sigma}$ in the actual configuration ${}^iV_k$ is given as

$$ {}^i\boldsymbol{\sigma} = {}^iJ^{-1}\,{}^i\mathbf{F}\,{}^i\mathbf{S}\,{}^i\mathbf{F}^T = {}^iJ^{-1}\,{}^i\mathbf{F}^0\mathbf{S}\,{}^i\mathbf{F}^T = {}^iJ^{-1}\,{}^i\mathbf{F}^0\boldsymbol{\sigma}\,{}^i\mathbf{F}^T, \tag{12} $$

where ${}^i\mathbf{F}$ is the deformation gradient describing the relationship between the original ${}^0\mathbf{X}$ and the actual ${}^i\mathbf{x}$ configurations, and ${}^iJ$ is the determinant of the deformation gradient, so ${}^iJ = det({}^i\mathbf{F})$.

$$ {}^i\mathbf{F} = \frac{\partial {}^i\mathbf{x}}{\partial {}^0\mathbf{X}}. \tag{13} $$

Because of the assumption of a zero increment of the second Piola–Kirchhoff stress tensor $\Delta\mathbf{S} = 0$, the first and second terms of the general equilibrium Eq. (3) are naturally zero, so the form-finding process is essentially linear. Thus, Eqs. (9)–(11) derived from the linearized form of virtual work variations blend with (3) completely and do not represent an approximation of the solution; instead, it represents a precise solution, as just proven theoretically. The form-finding problem turns into a linear analysis because of the assumptions described above.

To express the stress state of a particular finite element within its coordinate system, the co-rotational stress tensor ${}^i\overline{\boldsymbol{\sigma}}$ can be written down.

$$ {}^i\overline{\boldsymbol{\sigma}} = {}^iJ^{-1}\,{}^i\mathbf{U}\,{}^i\mathbf{S}\,{}^i\mathbf{U} = {}^iJ^{-1}\,{}^i\mathbf{U}^0\mathbf{S}\,{}^i\mathbf{U} = {}^i\mathbf{R}^{T\,0}\boldsymbol{\sigma}\,{}^i\mathbf{R}, \tag{14} $$

where ${}^i\mathbf{U}$ is the right stretch tensor, and ${}^i\mathbf{R}$ is the rotation tensor, obtained from the polar decomposition of the deformation gradient ${}^i\mathbf{F} = {}^i\mathbf{R}\,{}^i\mathbf{U}$. When looking at the co-rotational stress tensor ${}^i\overline{\boldsymbol{\sigma}}$, the relationship between the resulting stress state and the finite element stretching is obvious.

To demonstrate the results of the linear form-finding analysis utilizing stress density, the structure shown in Fig. 2 was calculated. Stress is defined in relation to the local coordinate systems of the finite elements, denoted by the right subscript l. The prestress values are ${}^0\boldsymbol{\sigma}_l = \{\sigma_x, \sigma_y, \tau_{xy}\}^T = \{1.00, 1.00, 0.00\}^T$ MPa, and the thickness of the membrane is $t = 0.001m$, which is used as the form-finding input. The stress transformation from the local to the global coordinate system used in Formula (12) is shown in Table 1. After solving the equilibrium equations described in (9)–(11), the resulting shape shown in Fig. 3 is obtained.

In conclusion, stress density is a robust stress adaptation procedure. It leads to a linearization of the form-finding analysis if stress densities are not adapted. However, this method is too strict in its linear form. The resulting stress state is obtained by mapping the initial stress state from the initial to the equilibrium configuration. As criticized in various studies [4,17], the resulting stress state is not usually feasible in construction, as it changes considerably over the structure and leads to stress concentrations, although in such cases, it is not physically needed. This unjustified stress concentration can be observed in the corners of the presented structure in Fig. 3. The stress concentration is necessary just near the hoop for conical membrane structures. Therefore, the resulting stress state can be considered non-optimal.

Moreover, when defining the initial stress ${}^0\boldsymbol{\sigma}$ in the initial configuration ${}^0V$, the resulting stress state ${}^i\boldsymbol{\sigma}$ in the actual configuration ${}^iV$ is dependent on the initial shape of the structure. On the other hand, when defining the relationship between stress and the element size, which are especially used as force densities for cable net structures, the resulting stress ${}^i\boldsymbol{\sigma}$ in the actual configuration ${}^iV$ is dependent on the FE discretization within the structure, which can be evaluated as an undesirable feature.

A possible modification to decrease the stress concentrations over the membrane structures is the application of stress density in nonlinear form [5,6,29]. If the nonlinear stress density concept is applied, then the stress ${}^0\boldsymbol{\sigma}$ is applied in a chosen number of iterations of form-finding analysis n. Therefore, while $i < n$, ${}^i\overline{\boldsymbol{\sigma}} = {}^0\boldsymbol{\sigma}$ is not obtained using the push-forward operation. The resulting stress state over the structure ${}^iV$ for the iteration $i = n$ is given by the push-forward operation described in Formula (12). The important distinction is the fact that the deformation gradient maps the deformation between the actual configuration ${}^iV$ and the previous configuration ${}^{i-1}V$ of the structure.

$$ {}^i_{i-1}\mathbf{F} = \frac{\partial {}^i\mathbf{x}}{\partial {}^{i-1}\mathbf{x}}. \tag{15} $$

Therefore, the difference between the linear and nonlinear SDMs can be seen when comparing Formulas (13) and (15).

Although this procedure usually results in smoother stress distribution over the structures, it principally removes the stress adaptations while performing iterations $i < n$ of the form-finding analysis. Thus, in the case of structures susceptible to shape diverging, collapsing, and mesh distorting, form-finding analysis leads to unsatisfactory results. To demonstrate the described behavior, a case study is shown in Fig. 4. Nonlinear stress density application was performed in three cases: (a) $n = 2$, (b) $n = 3$, and (c) $n = 4$. It can be observed that, although the concentration in the corners is decreasing, the shape is collapsing. According to Marbaniang et al. [29], "Iteratively updating the densities for non-minimal shapes ... causes convergence and mesh distortion issues".

2.3.2. Distortion control

The second stress adaptation procedure described here is called distortion control, which can be seen as a special case of element size control. This method was introduced by Bletzinger et al. [1,7–9]. Element size control introduces the maximal allowable configuration that can be reached by a finite element, while distortion control introduces the maximal allowable stretches instead. Recall the definition in [1]: "At the end of each form-finding step, the principal stretches, which are caused by the total deformation from the very first starting geometry to the actual intermediate solution, are evaluated for every point of the structure. If at least one of these stretches has a value beyond the allowed range, the target prestress is changed locally to enable equilibrium".

While the distortion control stress adaptation scheme is used within form-finding analysis, the prescribed stress is not modified until reaching the maximum allowed stretch in step $i = l$, where l denotes the configuration of reaching the limit value for a particular finite element. Before exceeding the maximal allowable deformation $0 < i < l$, the Cauchy stress tensor within the actual configuration is not obtained using the push-forward operation, as in the case of the linear SDM; thus, the form-finding process is principally nonlinear. As soon as the maximum allowed deformation is exceeded in step $i = l$ for a particular finite element, the push-forward operation applies to stress modifications within the actual configuration of the particular finite element. Thus, stress density is adopted upon reaching this limit state. It is important to emphasize that the step of exceeding the maximum allowed deformation differs for individual finite elements in general.

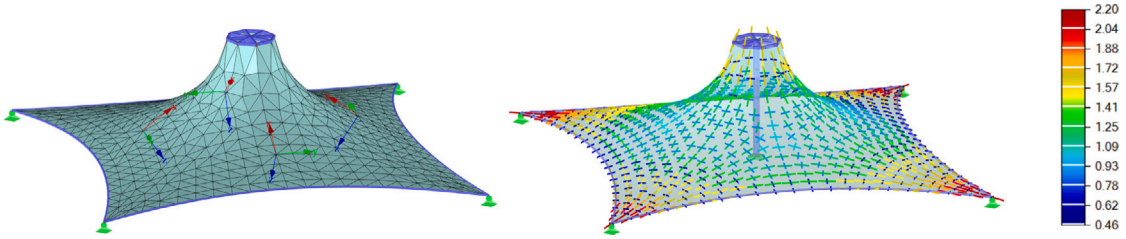

Fig. 3. Equilibrium shape (left) and vectors of principal forces n_1 and n_2 [kN/m] (right) for the linear stress density method.

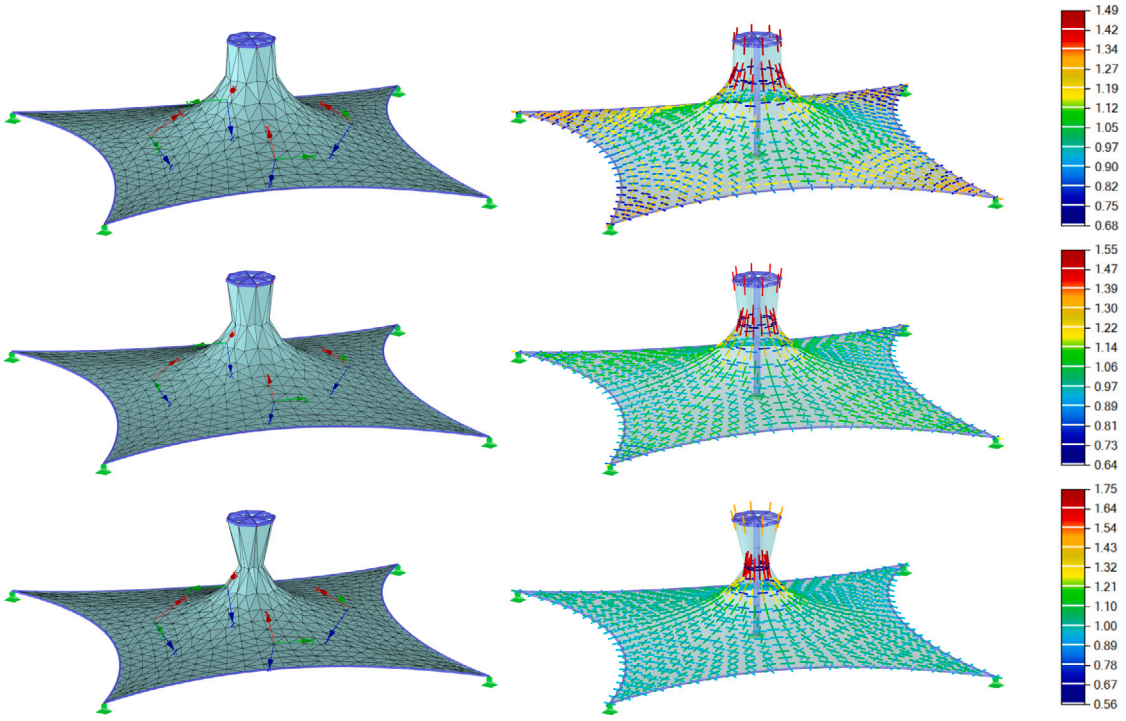

Fig. 4. Equilibrium shape and vectors of principal forces n_1 and n_2 [kN/m] for the nonlinear stress density method (from the top: $n = 2$, $n = 3$, $n = 4$).

During the form-finding analysis, the stress state prescribed by an engineer in the local coordinate systems of the finite elements is unchanged in step $i < l$. When the critical stretch reaches $i = l$, the actual stress ${}^{l}\boldsymbol{\sigma}_l$ is obtained using the push-forward operation between limit configuration ${}^{l}V_k$ and previous configuration ${}^{l-1}V_k$ [1]. To keep a consistent notation within this study, we assume performing the transformation of the stress tensor related to the local coordinate system ${}^{l}\boldsymbol{\sigma}_l$ to the global coordinate system, as described in Table 1. Thus, the Cauchy stress tensor ${}^{l}\boldsymbol{\sigma}$ is given for the subsequent push-forward operation. The Cauchy stress tensor ${}^{i}\boldsymbol{\sigma}$ in the actual configuration in step $i > l$ is given as

$$ {}^{i}\boldsymbol{\sigma} = {}^{i}_{l}J^{-1}\,{}^{i}_{l}\mathbf{F}\,{}^{l}\boldsymbol{\sigma}\,{}^{i}_{l}\mathbf{F}^{T}. \tag{16} $$

where the deformation gradient ${}^{i}_{l}\mathbf{F}$ describes the relationship between the actual configuration ${}^{i}\mathbf{x}$ and the limit configuration ${}^{l}\mathbf{x}$ in step l, as denoted by the addition of the left subscript. Furthermore, ${}^{i}_{l}J$ is the determinant of the deformation gradient ${}^{i}_{l}\mathbf{F}$.

$$ {}^{i}_{l}\mathbf{F} = \frac{\partial {}^{i}\mathbf{x}}{\partial {}^{l}\mathbf{x}}. \tag{17} $$

To demonstrate the results of the stress adaptation procedure described above, the structure shown in Fig. 2 was calculated. The same definition of prestress in the local coordinate system applies ${}^{0}\boldsymbol{\sigma}_l = \{\sigma_x, \sigma_y, \tau_{xy}\}^T = \{1.00, 1.00, 0.00\}^T$ MPa. Moreover, the ratio of the maximum allowable main stretches is defined as $\lambda = 1.05$. Considering ${}^{i}_{l}U_1$ and ${}^{i}_{l}U_2$ as the main stretches of the right stretch tensor ${}^{i}_{l}\mathbf{U}$, which correspond to the deformations of the membrane finite element, the force modifications are introduced, provided that the condition ${}^{i}_{l}U_1 \vee {}^{i}_{l}U_2 \notin \langle 1/\lambda, \lambda \rangle$ is valid [1]. The resulting equilibrium shape and the final stresses are shown in Fig. 5. When comparing the results presented in Figs. 3 and 5, we can see that a slightly smoother stress distribution was obtained, which is closer to the predefined values over the structure. While the maximal allowable stretch is increased, the stress concentrations in the corners decrease and the mesh distortions increase, manifesting by gradual collapsing of the cone-like membrane structure.

The principal assumption of distortion control is described briefly here. Further information can be found in the studies by Bletzinger et al. [1,7–9], including other variations of this method formulation but without changing the essential principle described above.

2.3.3. Further remarks on existing methods

Two mapping-based stress adaptation schemes that are independent of the material are presented. They are used later for a comparison with the proposed stress projection adaptation scheme to describe their principal differences and to explain the reason for the unique behavior of the proposed scheme. Both stress adaptation schemes lead to reaching the equilibrium shapes within the form-finding analysis, so the resulting stresses shown in Figs. 3 and 5 can be evaluated.

A justified requirement when performing form-finding analysis is obtaining well-distributed stress over the membrane structure without unnecessary concentrations. While stress density is applied in linear

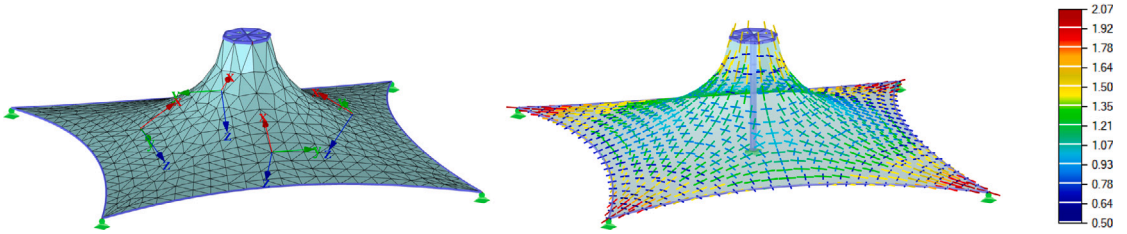

Fig. 5. Equilibrium shape and vectors of principal forces n_1 and n_2 [kN/m] for distortion control with $\lambda = 1.05$.

form, form-finding usually leads to the production of unnecessary overstressed regions over the structures. While stress density is utilized in a nonlinear manner or in distortion control, form-finding leads to well-distributed prestresses for many membrane structures. However, both methods suffer when conical shapes are solved.

Conical membrane structures differ fundamentally, as these shapes require stress concentrations near the hoop, while stress concentrations in the corners of the base are unnecessary. Strongly adapting the prescribed prestress in the top area of such structures is required to avoid necking. When stress density is applied in a nonlinear manner, the conical membranes suffer from collapse, as presented above. When distortion control is utilized, on–off switching, which is needed to decide whether the stresses need to be modified, leads to an uncontrolled sliding of nodes before stabilization is activated. This causes problems in the top parts of the conical membrane structures, and the ratio of the maximum allowable main stretches λ must be quite small.

Moreover, neither of the above methods automatically distinguish between different parts of the structure. When these stress adaptation schemes are applied to the conical membrane structure shown in Fig. 2, undesirable concentrations in the corner parts of the structure appear (see Fig. 5). These concentrations are only physically needed near the hoop, while a rather smooth distribution would be more favorable in corner areas. To avoid this problem, stress projection is proposed, which is especially designed for the conical type of membrane structure.

3. The proposed stress projection procedure

The proposed stress projection is a stress adaptation procedure intended especially for conical membrane structures. Generally, the process consists of three steps. First, a projection plane is defined, in which the actual configuration of the structure is orthogonally projected onto. The selected projection plane is used as a fictitious plane, as it is different from the inertial frame and the Eulerian frame. Second, the stress state within the projection plane is determined.

Finally, the stress states in the actual configuration of the membrane structure are derived using the composition quantity of the deformation gradients, computed on the fictitious configuration and thus using the coordination transformation operator from the projection plane to the initial one. Note that the element shapes projected on the projection plane usually change during iterations. It will be shown that the proposed method significantly improves acute stress formation in the top areas of the conical membranes, while stress formation in the flat zones tends to be negligible. Thus, the proposed method avoids the strangulation of conical membrane structures, as illustrated in Fig. 2, and leads to a smoothly distributed general anisotropic prestress.

Furthermore, in case the equilibrium is defined within the projection plane, the proposed method features the total independence of the final equilibrium shape and its FE discretization, as well as the shape of the initial structure configuration, which is a unique behavior. Next, a detailed description of the proposed stress projection is presented.

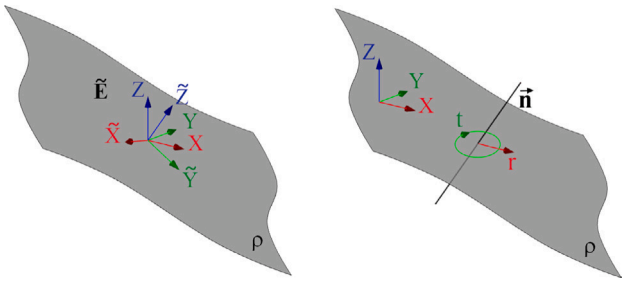

Fig. 6. Projection plane ρ given by base $\tilde{\mathbf{o}}$ and associated with axes $\tilde{x}$ and $\tilde{y}$ (left), projection plane ρ given by oriented line $\vec{\mathbf{n}}$ and associated with axes $\tilde{r}$ and $\tilde{t}$ (right).

3.1. Kinematics relations within stress projection

First, the kinematics relations used in stress projection are described, which are used later for the stress transformations. The arbitrarily oriented projection plane ρ is determined by defining its base $\tilde{\mathbf{O}}$ or an oriented line $\vec{\mathbf{n}}$, as shown in Fig. 6. Note that the base $\tilde{\mathbf{O}}$ applies if an orthogonal stress arrangement within the projection plane is required, while the oriented line $\vec{\mathbf{n}}$ applies if a radial stress arrangement within the projection plane is required, as will be described later.

Fig. 7 illustrates the actual configuration of the highlighted finite element in the initial configuration ${}^0V$ in step $i = 0$ and then ${}^iV$ in step i. The prestresses in the spatial configurations ${}^0V$ and ${}^iV$ are derived based on the prestress defined in projection plane ρ. The fictitious configurations ${}^0\tilde{V}$ and ${}^i\tilde{V}$ within projection plane ρ are obtained using an orthogonal projection of the spatial configuration onto the projection plane:

$$ {}^0P : {}^0V \to {}^0\tilde{V}, \quad {}^iP : {}^iV \to {}^i\tilde{V}, \tag{18} $$

where $\{{}^0P :\}$ and $\{{}^iP :\}$ indicate the orthogonal projection of ${}^0V$ and ${}^iV$ onto the associated projection plane ρ, leading to their fictitious reference configurations ${}^0\tilde{V}$ and ${}^i\tilde{V}$ in steps $i = 0$ and i, respectively. Note that the fictitious quantities are always indicated by a tilde in the text below.

The kinematic relations are derived based on the actual configurations ${}^0V$ and ${}^iV$ in step $i = 0$ and the next step i, as well as on the fictitious reference configurations ${}^0\tilde{V}$ and ${}^i\tilde{V}$. Thus, the fictitious deformation gradient ${}^0\tilde{\mathbf{F}}$ and ${}^i\tilde{\mathbf{F}}$ can be described as

$$ {}^0\tilde{\mathbf{F}} = \frac{\partial {}^0\mathbf{X}}{\partial {}^0\tilde{\mathbf{X}}} = \begin{bmatrix} \frac{\partial {}^0x}{\partial {}^0\tilde{X}} & \frac{\partial {}^0x}{\partial {}^0\tilde{Y}} & \frac{\partial {}^0x}{\partial {}^0\tilde{Z}} \\ \frac{\partial {}^0y}{\partial {}^0\tilde{X}} & \frac{\partial {}^0y}{\partial {}^0\tilde{Y}} & \frac{\partial {}^0y}{\partial {}^0\tilde{Z}} \\ \frac{\partial {}^0z}{\partial {}^0\tilde{X}} & \frac{\partial {}^0z}{\partial {}^0\tilde{Y}} & \frac{\partial {}^0z}{\partial {}^0\tilde{Z}} \end{bmatrix}, \quad {}^i\tilde{\mathbf{F}} = \frac{\partial {}^i\mathbf{x}}{\partial {}^i\tilde{\mathbf{X}}} = \begin{bmatrix} \frac{\partial {}^ix}{\partial {}^i\tilde{X}} & \frac{\partial {}^ix}{\partial {}^i\tilde{Y}} & \frac{\partial {}^ix}{\partial {}^i\tilde{Z}} \\ \frac{\partial {}^iy}{\partial {}^i\tilde{X}} & \frac{\partial {}^iy}{\partial {}^i\tilde{Y}} & \frac{\partial {}^iy}{\partial {}^i\tilde{Z}} \\ \frac{\partial {}^iz}{\partial {}^i\tilde{X}} & \frac{\partial {}^iz}{\partial {}^i\tilde{Y}} & \frac{\partial {}^iz}{\partial {}^i\tilde{Z}} \end{bmatrix}, \tag{19} $$

where ${}^0\mathbf{X}$ and ${}^i\mathbf{x}$ describe the actual configurations ${}^0V$ and ${}^iV$ in the initial step $i = 0$ and in step i, and ${}^0\tilde{\mathbf{X}}$ and ${}^i\tilde{\mathbf{X}}$ describe the fictitious configurations ${}^0\tilde{V}$ and ${}^i\tilde{V}$, which can be viewed as orthogonal projections of ${}^0V$ and ${}^iV$ according to Eq. (18).

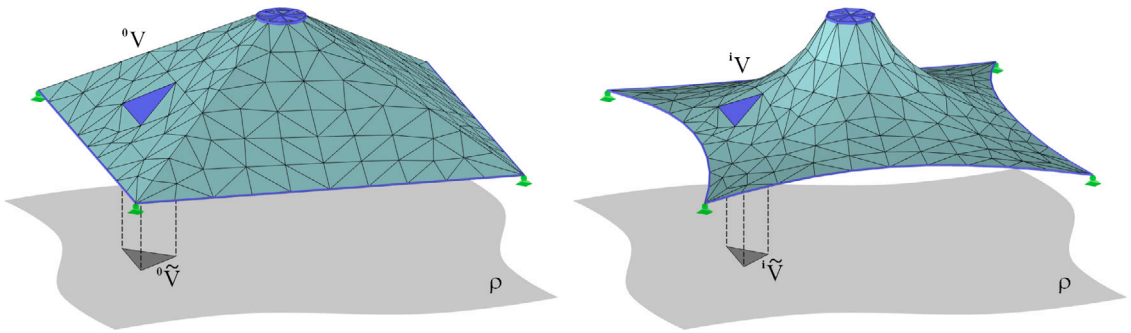

Fig. 7. Real and fictitious reference configurations in steps $i = 0$ and i.

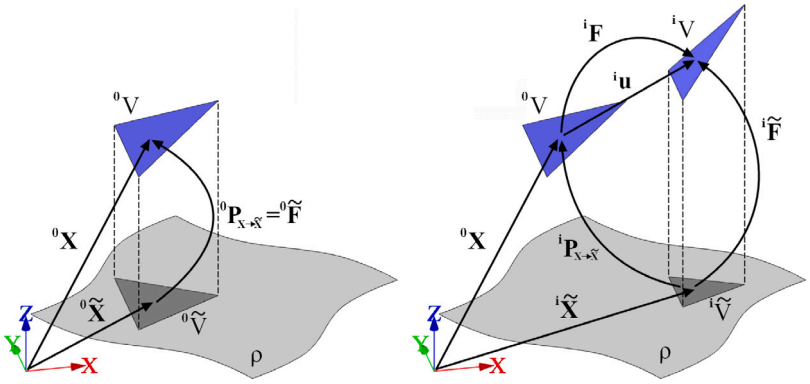

Fig. 8. Kinematics relations in steps $i = 0$ (left) and i (right).

Applying the chain rule, the relationships (19) can be modified into the following form:

$$
\begin{aligned}
{}^{0}\tilde{\mathbf{F}} &= \frac{\partial {}^{0}\mathbf{X}}{\partial {}^{0}\tilde{\mathbf{X}}} \frac{\partial {}^{0}\mathbf{X}}{\partial {}^{0}\mathbf{X}} = {}^{0}\mathbf{P}_{X\to\tilde{X}}\,{}^{0}\mathbf{F} = {}^{0}\mathbf{P}_{X\to\tilde{X}}\mathbf{I} = {}^{0}\mathbf{P}_{X\to\tilde{X}}, \\
{}^{i}\tilde{\mathbf{F}} &= \frac{\partial {}^{0}\mathbf{X}}{\partial {}^{i}\tilde{\mathbf{X}}} \frac{\partial {}^{i}\mathbf{x}}{\partial {}^{0}\mathbf{X}} = {}^{i}\mathbf{P}_{X\to\tilde{X}}\,{}^{i}\mathbf{F},
\end{aligned}
\tag{20}
$$

where ${}^{0}\mathbf{F}$ and ${}^{i}\mathbf{F}$ are the standard formulations of the deformation gradient performed for steps $i = 0$ and i, and ${}^{0}\mathbf{P}_{X\to\tilde{X}}$ and ${}^{i}\mathbf{P}_{X\to\tilde{X}}$ are the projection operators that transform the standard deformation gradient into the fictitious projection deformation gradients ${}^{0}\tilde{\mathbf{F}}$ and ${}^{i}\tilde{\mathbf{F}}$, as shown in Fig. 8. In the original configuration of the structure, the deformation gradient ${}^{0}\mathbf{F}$ apparently corresponds to identity matrix $\mathbf{I}$, and the fictitious deformation gradient ${}^{0}\tilde{\mathbf{F}}$ corresponds to the projection operator ${}^{0}\mathbf{P}_{X\to\tilde{X}}$.

The projection operators ${}^{0}\mathbf{P}_{X\to\tilde{X}}$ and ${}^{i}\mathbf{P}_{X\to\tilde{X}}$ change during the analysis and are the true sources of the absolute independence between fictitious deformation gradients ${}^{0}\tilde{\mathbf{F}}$ resp. ${}^{i}\tilde{\mathbf{F}}$ and the original configuration. This is why the proposed stress projection procedure results in independence between the initial and equilibrium shapes. Instead, the stress projection adaptation scheme defines the interdependence between the chosen projection plane and the equilibrium shape.

In other words, the defined projection plane determines the shape of the projected finite element, which is utilized to evaluate a fictitious deformation gradient. This fictitious deformation gradient, which is no longer related to the initial configuration but to the chosen projection plane, is further applied to the stress mapping process, as described above.

Note that the description above refers to the actual configurations ${}^{0}V$ and ${}^{i}V$ in two different calculation steps $i = 0$ and i. This was done to emphasize that such a procedure is performed in every configuration during the form-finding analysis $i = 0, \ldots, i-1, i, i+1 \ldots$, even for the initial configuration ${}^{0}V$, which is associated with the fictitious reference configuration ${}^{0}\tilde{V}$ used for the stress state estimation. Having emphasized this really important situation, only the generalized step i is used in the following text, but the procedures are valid for step $i = 0$ and every other step.

3.2. Equilibrium within the projection plane

An arbitrarily oriented projection plane ρ is determined using its base $\tilde{\mathbf{O}}$ or an oriented line $\vec{\mathbf{n}}$. Furthermore, equilibrium stress is determined within plane ρ. Note that there is no reference to the structure now but only to the equilibrium stress field in unbounded projection plane ρ.

If the orthogonal stress arrangement within the projection pane is required, the base $\tilde{\mathbf{O}}$ is needed to define the orientation and coordinate system of such a plane. Furthermore, specifying prestress values is necessary to determine the stationary stress state $\tilde{\mathbf{S}}_{\rho}$ within the unbounded projection plane ρ:

$$
\tilde{\mathbf{S}}_{\rho} = \{\tilde{S}_{\tilde{X}}, \tilde{S}_{\tilde{Y}}, \tilde{S}_{\tilde{X}\tilde{Y}}\}^{T}, \tag{21}
$$

where $\tilde{\mathbf{S}}_{\rho}$ is the stress field in vector form associated with the coordinate system given by $\tilde{\mathbf{O}}$. The stress field $\tilde{\mathbf{S}}_{\rho}$ is generally given by the definition of the prestress values $\tilde{S}_{\tilde{X}}$, $\tilde{S}_{\tilde{Y}}$, and $\tilde{S}_{\tilde{X}\tilde{Y}}$ as input for the form-finding analysis. Isotropic and constant orthogonal anisotropic prestress can exist in projection plane ρ, as the requirement for a zero Gaussian curvature is fulfilled. Fig. 9 shows an example of a segment of the unbounded projection plane ρ with $\tilde{\mathbf{S}}_{\rho} = \{1.50, 1.00, 0.00\}^{T}$ MPa on the left side.

Furthermore, if a radial stress arrangement is required, specifying an oriented line $\vec{\mathbf{n}}$ is necessary. This oriented line defines both the orientation of the projection plane ρ and the center of the radially arranged field of stresses in equilibrium. Again, it is necessary to emphasize that the prestress over the unbounded projection plane is assumed now, but not the structure. Moreover, a constant anisotropic prestress cannot exist within such a prestress arrangement, so a general

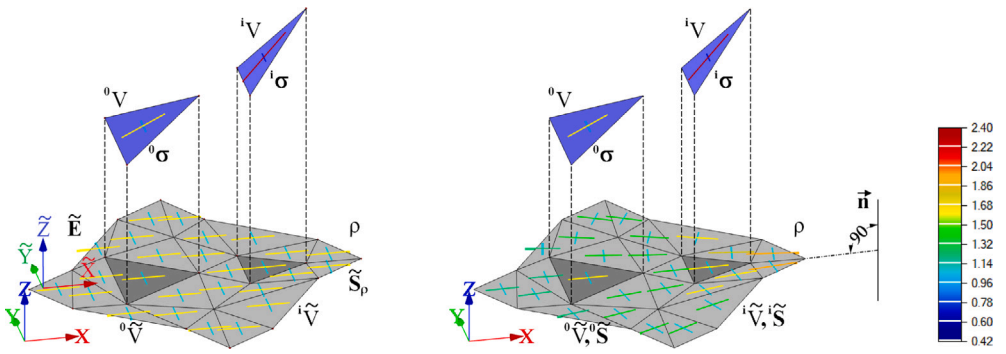

Fig. 9. Orthogonal (left) and radial (right) equilibrium stress states within the segment of the unbounded projection plane ρ. stress in spatial configurations derived from equilibrium in projection plane ρ.

anisotropic prestress needs to be determined based on two defined values:

$$\tilde{\mathbf{S}}_\rho = f(\tilde{S}_{\tilde{r}}, \tilde{S}_{\tilde{t}}), \tag{22}$$

where $\tilde{S}_{\tilde{r}}$ and $\tilde{S}_{\tilde{t}}$ are the input values of the form-finding analysis in a specific distance d from the oriented line $\vec{\mathbf{n}}$ (see Fig. 9), which are associated with the polar coordinate system axes $\tilde{r}$ and $\tilde{t}$. Assuming that the values $\tilde{S}_{\tilde{r}}$ and $\tilde{S}_{\tilde{t}}$ are given, the equilibrium anisotropic stress field $\tilde{\mathbf{S}}_\rho$ within the unbounded projection plane can be determined analytically, as will be presented later. While the implementation of stress projection into the form-finding analysis it is not necessary to enter a distance d. It could be determined automatically in such a way that the defined stress values $\tilde{S}_{\tilde{r}}$ and $\tilde{S}_{\tilde{t}}$ are the mean values within the area given by the projection of the membrane structure onto the projection plane. Fig. 9 shows an example of a segment of the projection plane ρ, where $\tilde{\mathbf{S}}_\rho = f(1.50, 1.00)$ MPa, and d is determined automatically.

An equilibrium stress $\tilde{\mathbf{S}}_\rho$ within the unbounded projection plane ρ is determined. Assuming this stress field is generally anisotropic, the second Piola–Kirchhoff stress tensor ${}^i\tilde{\mathbf{S}}_\rho$ associated with the fictitious reference configuration ${}^i\tilde{V}_\rho$ of a particular finite element in step i is not constant, but it depends on the actual position within the projection plane ρ (see Fig. 7). Thus, it can be written as

$${}^i\tilde{\mathbf{S}}_\rho = f(\tilde{\mathbf{S}}_\rho, {}^i\tilde{V}_\rho), \tag{23}$$

where $\tilde{\mathbf{S}}_\rho$ is the equilibrium in the unbounded projection plane, and ${}^i\tilde{\mathbf{S}}_\rho$ is the second Piola–Kirchhoff stress tensor associated with the fictitious reference configuration ${}^i\tilde{V}_\rho$ in step i. The quantities are described with respect to the base $\tilde{\mathbf{O}}$ of the projection plane ρ, as indicated by the right subscript. The base $\tilde{\mathbf{O}}$ can be specified directly or derived from the defined oriented line $\vec{\mathbf{n}}$.

To keep the equations consistent with the methods described above, the procedure for estimating stresses within the structure is described with regard to the global Cartesian coordinate system, which is used for assembling the equilibrium equations described in Eqs. (9)–(11), as indicated by the missing right subscript. Thus, the second Piola–Kirchhoff stress tensor ${}^i\tilde{\mathbf{S}}_\rho$ is transformed into ${}^i\tilde{\mathbf{S}}$:

$${}^i\tilde{\mathbf{S}} = \mathbf{R}_g\, {}^i\tilde{\mathbf{S}}_\rho \mathbf{R}_g^T, \tag{24}$$

$$\mathbf{R}_g = \mathbf{O} \otimes \tilde{\mathbf{O}} = \begin{bmatrix} c_{X\tilde{X}} & c_{X\tilde{Y}} & c_{X\tilde{Z}} \\ c_{Y\tilde{X}} & c_{Y\tilde{Y}} & c_{Y\tilde{Z}} \\ c_{Z\tilde{X}} & c_{Z\tilde{Y}} & c_{Z\tilde{Z}} \end{bmatrix}, \tag{25}$$

where $c_{X\tilde{X}}$ denotes the cosine between the vectors X and $\tilde{X}$ of the global Cartesian coordinate system and the coordinate system of the projection plane ρ. Furthermore, $\mathbf{O}$ and $\tilde{\mathbf{O}}$ are the bases of the global Cartesian coordinate system and the coordinate system of the projection plane ρ, respectively. Thus, $\mathbf{R}_g$ is the rotation matrix for the transformation between both coordinate systems.

3.3. Stress state within the structure

A stress state, described by the second Piola–Kirchhoff stress tensor ${}^i\tilde{\mathbf{S}}$ within the fictitious reference configuration ${}^i\tilde{V}$ in step i, was obtained in Eq. (24). Utilizing the fictitious deformation gradient ${}^i\tilde{\mathbf{F}}$ (Eq. (20)), the push-forward operation is performed to estimate the Cauchy stress tensor ${}^i\boldsymbol{\sigma}$ within the actual configuration ${}^iV$ in step i:

$${}^i\boldsymbol{\sigma} = {}^i\tilde{J}^{-1}\, {}^i\tilde{\mathbf{F}}\, {}^i\tilde{\mathbf{S}}\, {}^i\tilde{\mathbf{F}}^T, \tag{26}$$

where ${}^i\tilde{J}$ is the determinant of the fictitious deformation gradient ${}^i\tilde{\mathbf{F}}$. The process is shown in Fig. 9.

Furthermore, the stress state within the highlighted finite element is shown numerically in Fig. 9, presenting the estimation within projection plane ρ. The stress state shown is related to both the initial configuration ${}^0V$ and the actual configuration ${}^iV$ of a particular finite element moving in the space within the form-finding analysis.

Using Eq. (26) for the solution of form-finding analysis described in Eqs. (9)–(11) and considering the configuration ${}^iV$ in step i, a new configuration ${}^{i+1}V$ of the structure is obtained. The same procedure of the stress estimation is performed, which gives the fictitious reference configuration ${}^{i+1}\tilde{V}$ obtained by an orthogonal projection of ${}^{i+1}V$ onto the projection plane. Furthermore, a new fictitious deformation gradient ${}^{i+1}\tilde{\mathbf{F}}$ and the second Piola–Kirchhoff stress tensor ${}^{i+1}\tilde{\mathbf{S}}$ are determined. Thus, the Cauchy stress tensor in step $i+1$ is given as

$${}^{i+1}\boldsymbol{\sigma} = {}^{i+1}\tilde{J}^{-1}\, {}^{i+1}\tilde{\mathbf{F}}\, {}^{i+1}\tilde{\mathbf{S}}\, {}^{i+1}\tilde{\mathbf{F}}^T. \tag{27}$$

Following this procedure, the structure converges to the equilibrium shape. There is no dependency between the stress state within steps i and $i+1$ at all, and the resulting equilibrium shape does not depend on the initial configuration or FE discretization.

3.4. Determining equilibrium within a polar coordinate system

For stress projection, determining the equilibrium in the projection plane, as described above, is necessary. In addition to isotropic prestress, a constant anisotropic prestress can be used because the Gaussian curvature equals zero. For conical membrane structures, however, the prestress defined in the polar coordinate system is of high importance. In such an arrangement, constant anisotropic prestress cannot exist. Therefore, determining a general anisotropic stress field $\tilde{\mathbf{S}}_\rho$ based on two input values is necessary. The oriented line $\vec{\mathbf{n}}$ determines both the orientation of the projection plane in space and the center of the polar coordinate system.

To determine the equilibrium in the polar coordinate system, a fictitious infinitesimal segment of the projection plane ρ is assumed, described by its length Δr and angle $\Delta\alpha$, as shown in Fig. 10. This segment does not correspond to any finite element or its projection, but it is just an imaginary segment used for the definition of general anisotropic equilibrium $\tilde{\mathbf{S}}_\rho$.

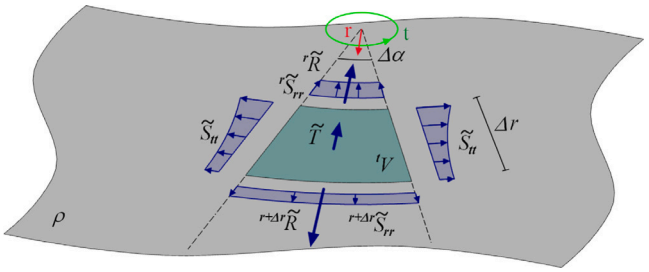

Fig. 10. Equilibrium of forces in the polar coordinate system within the projection plane.

The following estimation of the equilibrium within the projection plane uses index notation, so $\tilde{S}_{rr}$ and $\tilde{S}_{tt}$ represent the second Piola–Kirchhoff stresses in the radial and tangential directions, respectively. Assuming rotational symmetry, the shear stresses are equal to zero $\tilde{S}_{rt} = \tilde{S}_{tr} = 0$. In addition, the equilibrium in the tangential direction is met because of rotational symmetry. Thus, it is only necessary to satisfy the equilibrium in the radial direction, which is expressed by the resultants of radial stresses ${}^{r}\tilde{R}$ and ${}^{r+\Delta r}\tilde{R}$ in the positions r and $r + \Delta r$, and the resultant of the radial components of tangential stresses $\tilde{T}$.

$$ {}^{r}\tilde{R} = \int_{\Delta\alpha} {}^{r}\tilde{S}_{rr} r \, d\alpha = {}^{r}\tilde{S}_{rr} r \Delta\alpha, \tag{28} $$

$$ {}^{r+\Delta r}\tilde{R} = \int_{\Delta\alpha} {}^{r+\Delta r}\tilde{S}_{rr}(r+\Delta r) \, d\alpha = {}^{r+\Delta r}\tilde{S}_{rr}(r+\Delta r)\Delta\alpha, \tag{29} $$

$$ \tilde{T} = \iint_{\Delta\alpha\Delta r} \tilde{S}_{tt} k r \, dr \, d\alpha = \Delta\alpha \int_{\Delta r} \tilde{S}_{tt} \, dr, \tag{30} $$

where k is the curvature expressed as $k = 1/r$. The equation of the equilibrium in the radial direction to be satisfied over the fictitious infinitesimal segment can be expressed as

$$ {}^{r+\Delta r}\tilde{R} = {}^{r}\tilde{R} + \tilde{T}. \tag{31} $$

After substituting Eqs. (28)–(30) into Eq. (31), the following formula is obtained:

$$ \int_{\Delta r} \tilde{S}_{tt} \, dr = {}^{r+\Delta r}\tilde{S}_{rr}(r+\Delta r) - {}^{r}\tilde{S}_{rr} r. \tag{32} $$

Thus, the equation of equilibrium in the projection plane is described. To fulfill Eq. (32), different prestress functions can be generated. A suitable choice when $\tilde{S}_{rr} > \tilde{S}_{tt}$ is

$$ \tilde{S}_{rr} = \frac{a}{r} + b, \quad \tilde{S}_{tt} = b, \tag{33} $$

where a and b are the constants of the functions. Assuming the required stress values $\tilde{S}_{rr}$ and $\tilde{S}_{tt}$ in the position $r = d$ are specified as an input of the form-finding analysis, the constants a and b can be determined. Moreover, by considering the defined prestress values $\tilde{S}_{rr}$ and $\tilde{S}_{tt}$ as the mean values in the projection plane, the value of d can also be determined automatically. Thus, the only required input of the form-finding analysis using the radial prestress arrangement is the standard requirement for prestress definition $\tilde{S}_{rr}$ and $\tilde{S}_{tt}$, thus defining the prestress in equilibrium in the radial arrangement $\tilde{\mathbf{S}}_{\rho} = f(\tilde{S}_{\tilde{r}\tilde{r}}, \tilde{S}_{\tilde{t}\tilde{t}})$ and defining the oriented line $\vec{\mathbf{n}}$.

3.5. Implementation considerations

The stress field within the projection plane is determined with respect to the associated coordinate system, which is generally different from the global coordinate system used for Eqs. (9)–(11). Thus, performing the transformation, as mentioned above, is necessary.

Assuming the above-mentioned stress field $\tilde{\mathbf{S}}_{\rho}$ is related to the polar coordinate system and Eq. (24), the second Piola–Kirchhoff stress tensor ${}^{i}\tilde{\mathbf{S}}_{\rho}$ related to the fictitious reference configuration ${}^{i}\tilde{V}_{\rho}$ in step i can be determined. The tensor ${}^{i}\tilde{\mathbf{S}}_{\rho}$ consists of its main values in radial direction $\tilde{S}_{rr}$ and tangential direction $\tilde{S}_{tt}$. The rotation matrix ${}^{i}\mathbf{R}_{g}$ is determined as a tensor product of the base $\mathbf{O}$ of the stationary global coordinate system and the base ${}^{i}\tilde{\mathbf{O}}$ of the polar coordinate system in the position of a particular integration node of the solved finite element ${}^{i}\tilde{V}$. Note that the base of the coordinate system related to the projection plane is not stationary ${}^{i}\tilde{\mathbf{O}}$ for the radial arrangement

$$ {}^{i}\mathbf{R}_{g} = \mathbf{O} \otimes {}^{i}\tilde{\mathbf{O}} = \begin{bmatrix} {}^{i}c_{X\tilde{X}} & {}^{i}c_{X\tilde{Y}} & {}^{i}c_{X\tilde{Z}} \\ {}^{i}c_{Y\tilde{X}} & {}^{i}c_{Y\tilde{Y}} & {}^{i}c_{Y\tilde{Z}} \\ {}^{i}c_{Z\tilde{X}} & {}^{i}c_{Z\tilde{Y}} & {}^{i}c_{Z\tilde{Z}} \end{bmatrix}, \tag{34} $$

where ${}^{i}c_{X\tilde{X}}$ is the cosine between vectors X and $\tilde{X}$ of the global and polar coordinate systems. Although these systems are stationary in general, the base ${}^{i}\tilde{\mathbf{O}}$ within the actual integration node changes during the form-finding analysis because of the changing position of fictitious reference configurations ${}^{i}\tilde{V}$, as shown in Fig. 7. The base ${}^{i}\tilde{\mathbf{O}}$ in the position of each integration point always fulfills both requirements; that is, it points to the center of the polar coordinate system and complies with oriented line $\vec{\mathbf{n}}$.

Eventually, the second Piola–Kirchhoff stress tensor ${}^{i}\tilde{\mathbf{S}}_{\rho}$ related to the polar coordinate system is transformed to the second Piola–Kirchhoff stress tensor ${}^{i}\tilde{\mathbf{S}}$ related to the global coordinate system:

$$ {}^{i}\tilde{\mathbf{S}} = {}^{i}\mathbf{R}_{g} \, {}^{i}\tilde{\mathbf{S}}_{\rho} \, {}^{i}\mathbf{R}_{g}^{T}, \tag{35} $$

The second Piola–Kirchhoff stress tensor ${}^{i}\tilde{\mathbf{S}}$ obtained in this way is further used to determine the Cauchy stress tensor ${}^{i}\boldsymbol{\sigma}$ within the actual configuration ${}^{i}V$ of the particular finite element according to Eq. (26).

3.6. Comparisons with two existing stress adaptation procedures

In the following table, a comparison of the proposed stress projection with the stress density and distortion control stress adaptation procedures is provided. Essential differences between particular assumptions can be observed.

The variables included in Table 1 can be described as follows. $\tilde{S}_{\tilde{r}}$ and $\tilde{S}_{\tilde{t}}$ are the stress values related to the polar coordinate system within the given projection plane ρ, determined by oriented line $\vec{\mathbf{n}}$; $\tilde{S}_{\tilde{X}}$, $\tilde{S}_{\tilde{Y}}$ and $\tilde{S}_{\tilde{X}\tilde{Y}}$ are the stress values related to the Cartesian coordinate system of the given projection plane, determined by base $\tilde{\mathbf{O}}$; σ_x, σ_y, and τ_{xy} are the required prestress values related to the local coordinate system of particular finite elements; and λ is the ratio of the maximal allowable stretching.

In the case of stress densities applied in linear form, the resulting stress state refers to the initial configurations ${}^{0}\mathbf{X}$ in step $i = 0$. When distortion control is used, the resulting stress state refers to the intermediate limit configuration ${}^{l}\mathbf{X}$ in step $i = l$. When stress projection is considered, the stress state refers to fictitious configuration ${}^{i}\tilde{\mathbf{X}}$, which continuously changes during the form-finding analysis and is independent of the initial configuration of the structure. Therefore, the resulting stress state is derived exclusively from the predefined stress state within the projection plane.

3.7. Further remarks on the proposed stress projection

After a closer inspection, the following observations can be made for the stress projection. If the actual configuration ${}^{i}V$ of the particular finite element is parallel to projection plane ρ, the orthogonal projection $\{{}^{i}P : \}$ leads to a fictitious reference configuration ${}^{i}\tilde{V}$ that coincides with the rigid body motion of the actual configuration. Therefore, virtual deformation gradient ${}^{i}\tilde{\mathbf{F}}$ is a unit matrix; ${}^{i}\tilde{\mathbf{F}} = \mathbf{I}$. The stress state ${}^{i}\boldsymbol{\sigma}$ within the actual configuration ${}^{i}V$ is equal to the stress state ${}^{i}\tilde{\mathbf{S}}$ within the fictitious reference configuration ${}^{i}\tilde{V}$.

On the other hand, if the inclination of the particular finite element ${}^{i}V$ is significant, the orthogonal projection $\{{}^{i}P : \}$ leads to the virtual reference configuration ${}^{i}\tilde{V}$, which differs considerably from the actual configuration ${}^{i}V$. Using the virtual deformation gradient ${}^{i}\tilde{\mathbf{F}}$, the

Table 1
Comparison of stress adaptation procedures.

Stress adaptation procedure	Stress projection (SP)	Stress density (SD)	Distortion control (DC)
Required input	$a)\tilde{S}_{\tilde{r}}, \tilde{S}_{\tilde{t}}, \vec{\mathbf{n}}$ $b)\tilde{S}_{\tilde{X}}, \tilde{S}_{\tilde{Y}}, \tilde{S}_{\tilde{X}\tilde{Y}}, \tilde{O}$	$\sigma_x, \sigma_y, \tau_{xy}$	$\sigma_x, \sigma_y, \tau_{xy}, \lambda$
Input stress	$a)^i\tilde{S}_\rho = f(\tilde{S}_\rho, {}^i\tilde{V}_\rho)$ $b)^i\tilde{S}_\rho = \{\tilde{S}_{\tilde{X}}, \tilde{S}_{\tilde{Y}}, \tilde{S}_{\tilde{X}\tilde{Y}}\}^T$	${}^0\boldsymbol{\sigma}_l = \{\sigma_x, \sigma_y, \tau_{xy}\}^T$	${}^l\boldsymbol{\sigma}_l = \{\sigma_x, \sigma_y, \tau_{xy}\}^T$
Stress transformation	${}^i\tilde{S} = {}^i\mathbf{R}_g {}^i\tilde{S}_\rho {}^i\mathbf{R}_g^T$	${}^0\boldsymbol{\sigma} = {}^0\mathbf{R}_g {}^0\boldsymbol{\sigma}_l {}^0\mathbf{R}_g^T$	${}^l\boldsymbol{\sigma} = {}^l\mathbf{R}_g {}^l\boldsymbol{\sigma}_l {}^l\mathbf{R}_g^T$
Deformation gradient	${}^i\tilde{F} = \partial^i\mathbf{x}/\partial^i\tilde{X}$	${}^iF = \partial^i\mathbf{x}/\partial^0X$	${}^iF = \partial^i\mathbf{x}/\partial^l\mathbf{x}$
Resulting stress	${}^i\boldsymbol{\sigma} = {}^i\tilde{J}^{-1} {}^i\tilde{F} {}^i\tilde{S} {}^i\tilde{F}^T$	${}^i\boldsymbol{\sigma} = {}^iJ^{-1} {}^iF {}^0\boldsymbol{\sigma} {}^i\mathbf{F}^T$	${}^i\boldsymbol{\sigma} = {}^i_lJ^{-1} {}^i_lF {}^l\boldsymbol{\sigma} {}^i_l\mathbf{F}^T$

changes between the stress state ${}^i\tilde{\mathbf{S}}$ within the projection plane and ${}^i\boldsymbol{\sigma}$ within the actual configuration are substantial. Basically, the stress adaptations of the stress projection lead to an increase in the prestress in the slope direction and to a decrease in the prestress in the direction of the contour lines.

The preceding observations explain why stress projection is an efficient stress adaptation procedure for the form-finding analysis of conical membrane structures—it avoids the undesirable strangulation near the hoop, while the stress in flat areas is scarcely affected. Moreover, the proposed stress adaptation procedure can be utilized for the shape optimization of shell structures subjected to self-weight because the projection plane can be perpendicular to the gravitational acceleration direction.

The proposed method also leads to equilibrium shapes that are independent of the initial configuration and the FE discretization of the structure, which is a unique feature lacking in existing stress adaptation schemes.

4. Numerical examples

The following section presents numerical examples to demonstrate the efficiency of the proposed stress projection procedure. This stress adaptation scheme was proposed and developed within the company FEM consulting and implemented in its FEA calculation core [31]. As part of the FEA calculation core, this stress adaptation scheme was consequently implemented into the RF-FORM-FINDING add-on module of the widely used structural engineering software RFEM by Dlubal Software [32]. The following examples were carried out within this software; interested readers may find and download many other examples on the Dlubal Software website [33] for subsequent analysis and study, as well as other examples created to investigate the abilities of the proposed stress projection. There are also various customer projects available on the website [34].

4.1. Conical membrane structure

The first example deals with the conical membrane structure shown in Fig. 2, as presented above. Stress projection, distortion control, and stress density were utilized as the stress adaptation schemes. Prestress is defined in terms of a force per unit width $\tilde{\mathbf{n}}_\rho = t\tilde{\mathbf{S}}_\rho$, ${}^0\mathbf{n}_l = t\,{}^0\boldsymbol{\sigma}_l$, and ${}^l\mathbf{n}_l = t\,{}^l\boldsymbol{\sigma}_l$, where t is the thickness of the surface, rather than the stress values $\tilde{\mathbf{S}}_\rho$, ${}^0\boldsymbol{\sigma}_l$, and ${}^l\boldsymbol{\sigma}_l$, because this is the more common input manner for membrane structures. This, of course, does not change any of the above-mentioned relations, and the only intention of using this input is to apply the standardized way of work when performing the form-finding analysis.

An isotropic prestress was specified. The values $\tilde{n}_{\tilde{r}} = \tilde{n}_{\tilde{t}} = 1.00$ kN/m and $\tilde{n}_{\tilde{r}t} = 0.00$ kN/m, or $\tilde{\mathbf{n}}_\rho = \{1.00, 1.00, 0.00\}^T$ kN/m in a vector form were defined for the stress projection. The values $n_x = n_y = 1.00$ kN/m and $n_{xy} = 0.00$ kN/m or ${}^0\mathbf{n}_l = {}^l\mathbf{n}_l = \{1.00, 1.00, 0.00\}^T$ kN/m in a vector form were defined for both distortion control and stress density. The oriented line $\vec{\mathbf{n}} = \{0, 0, 1\}^T$ coincides with the Z axis of the global coordinate system and the middle of the hoop. For the parameter $\lambda = 1.05$, such a value is defined to avoid necking and in-plane mesh distortion over the conical membrane structure. By increasing the magnitude of λ, the resistance against the necking process decreases consequently. For stress density, utilization in linear form is considered to avoid necking, as presented in Fig. 4.

The initial shape of the membrane structure is defined by the base of the square shape with a side length of $l = 10.00$ m, supported by cables with the required resulting sag $s = 10.0$ % of their lengths at the end of the form-finding analysis. The cables are simply supported in the corners of the base. The hoop with a radius of $r = 0.60$ m is situated on the top of the cantilevered column with a height of $h = 3.00$ m. The resulting equilibrium shapes are shown in Fig. 11, and the principal internal forces are shown in Figs. 12–14.

Based on the presented results, the following can be concluded. All stress adaptation schemes led to equilibrium shapes. Incorporation of the stress projection resulted in a considerably different stress distribution over the structure, which exhibits no concentrations in the corners and generally a smoother distribution of stresses, which is highly desirable. The results when applying stress density exhibit a similar stress distribution as distortion control, as presented in Fig. 3.

Table 2 summarizes the prestress distributions over the example structure. The results are presented for all methods mentioned.

The values n_{1k} and n_{2k} are the principal forces in the finite elements, m is the total number of 2D finite elements over the membrane structure, and $\bar{n}_1$ and $\bar{n}_2$ are the average values of the principal forces.

$$\bar{n}_1 = \frac{1}{m}\sum_{k=1}^{m} n_{1k}, \quad \bar{n}_2 = \frac{1}{m}\sum_{k=1}^{m} n_{2k} \tag{36}$$

The uniform distribution would correspond with $|\Delta\bar{n}_1| = 0.00$ kN/m and $|\Delta\bar{n}_2| = 0.00$ kN/m; therefore, a lower sum of the absolute values of stress differences corresponds with a desirable lower level of stress concentrations. The values Δn_1^* and Δn_2^* express the deviation of the resulting average principal forces $\bar{n}_1$ and $\bar{n}_2$ from the input values described above, hence the difference from the intended values represented by the principal forces 1.00 kN/m. It is important to note that it is impossible for these structures to reach a uniform prestress distribution because the concentrations are inherent in the final shape around the hoop.

Stress density, distortion control, and other standard stress adaptation schemes modify the forces according to the deformations within the form-finding analysis and generally do not distinguish between different areas of the structure. On the other hand, the stress projection exhibits somewhat favorable smoother modifications because the resulting equilibrium is independent of the calculation path during the form-finding analysis; the equilibrium is derived exclusively from the predefined equilibrium in the projection plane. Therefore, stretching the finite elements in the corner parts does not lead to stress concentrations when using stress projection.

Stress concentration near the hoop is natural, where further stress increases emerge under loading cycles during the service duration of the structure. Therefore, these areas are often double layered. However, the concentrations in the corner parts are not physically needed and should be avoided, so the prestress redistribution shown in the figures above is indeed the most important benefit of the proposed stress projection.

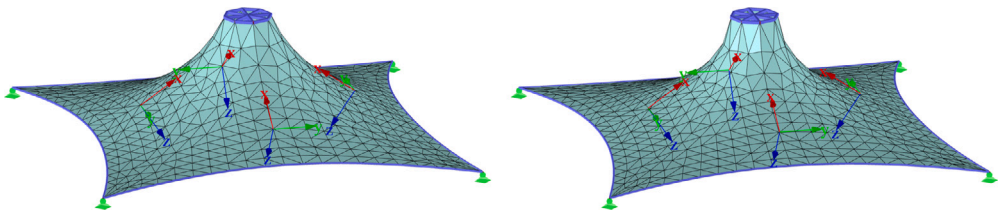

Fig. 11. Equilibrium Shapes using stress projection (left) and distortion control (right).

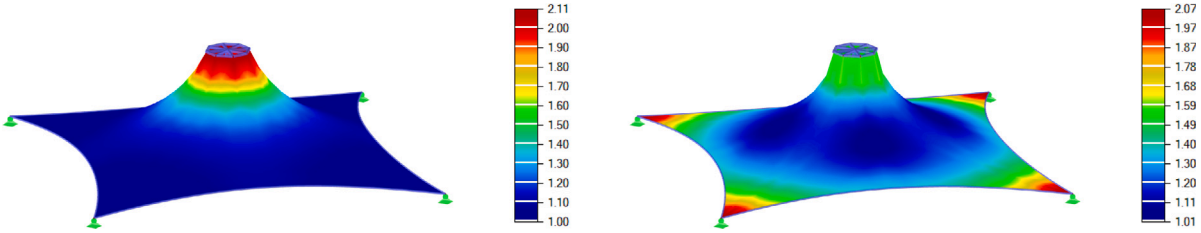

Fig. 12. First principal internal forces n_1 [kN/m] using stress projection (left) and distortion control (right).

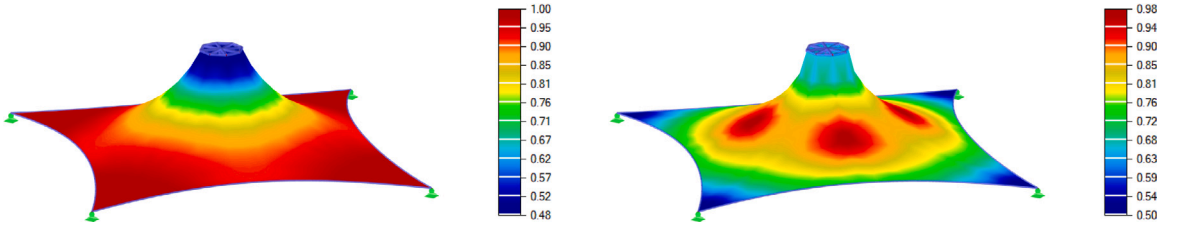

Fig. 13. Second principal internal forces n_2 [kN/m] using stress projection (left) and distortion control (right).

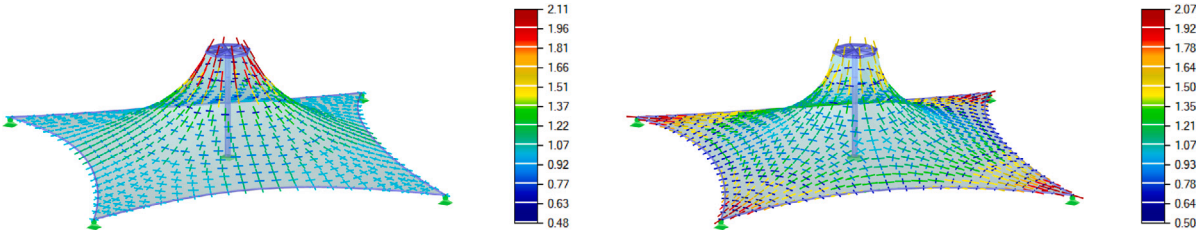

Fig. 14. Vectors of principal internal forces n_1 and n_2 [kN/m] using stress projection (left) and distortion control (right).

Table 2
Comparison of the utilized stress adaptation procedures.

Evaluated quantities	Unit	Stress projection (SP)	Distortion control (DC)	Stress density (SD)
$\bar{n}_1$	kN/m	1.14570	1.30518	1.37417
$\bar{n}_2$	kN/m	0.89174	0.78255	0.74977
$\lvert\Delta\bar{n}_1\rvert = \frac{1}{m}\sum_{k=1}^{m}\lvert n_{1k} - \bar{n}_1\rvert$	kN/m	0.12399 (≈ 10.82%)	0.15632 (≈ 11.98%)	0.19738 (≈ 14.36%)
$\lvert\Delta\bar{n}_2\rvert = \frac{1}{m}\sum_{i=k}^{m}\lvert n_{2k} - \bar{n}_2\rvert$	kN/m	0.07722 (≈ 8.66%)	0.08324 (≈ 10.64%)	0.09651 (≈ 12.87%)
$\Delta n_1^* = \bar{n}_1 - 1.00$	kN/m	0.14570 (≈ 14.57%)	0.30518 (≈ 30.52%)	0.37417 (≈ 37.42%)
$\Delta n_2^* = \bar{n}_2 - 1.00$	kN/m	−0.10826 (≈ −10.83%)	−0.21745 (≈ −21.75%)	−0.25023 (≈ −25.02%)

4.2. Initial shape independence of the stress projection algorithm

As claimed above, the proposed stress projection leads to independence between the initial and equilibrium configurations of the structure. This unique feature is a natural consequence of using the projected fictitious configuration within the form-finding analysis. Other existing stress adaptation schemes refer to a real deformation gradient, which implies the dependency of the final shape on its initial approximation or the intermediate configuration, as mentioned above. The behavior described is demonstrated in an example of the conical membrane structure used earlier, in which the initial configuration is modified quite strongly. In the following figures, the initial and final configurations can be observed (see Figs. 15–17). The prestress and boundary conditions are the same as in the previous example.

The projection plane in the example above is defined via the oriented line $\vec{\mathbf{n}} = \{0, 0, 1\}^T$, which coincides with the Z axis of the global coordinate system. Naturally, it is possible to use any definition of the oriented line, so the projection plane can be arbitrarily inclined, which has a significant impact on the resulting equilibrium within the structure designed in the form-finding analysis. This allows the structural engineer and architect to adapt the prestress distribution for the intended structure, which can be arbitrarily arranged in space.

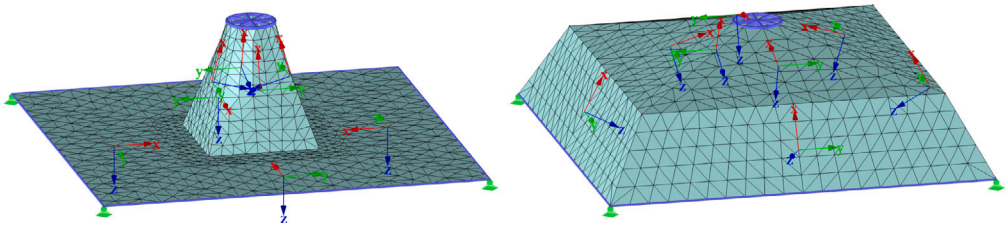

Fig. 15. Two different initial configurations of the conical membrane structure.

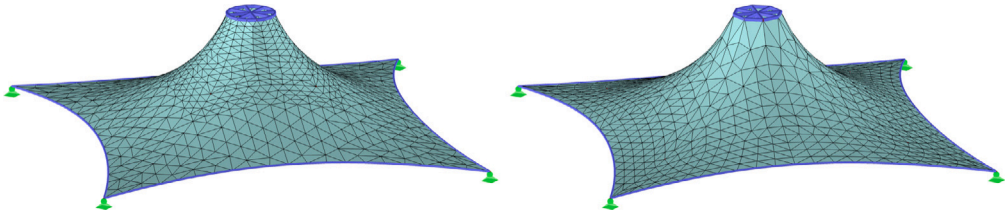

Fig. 16. Equilibrium shapes for stress projection.

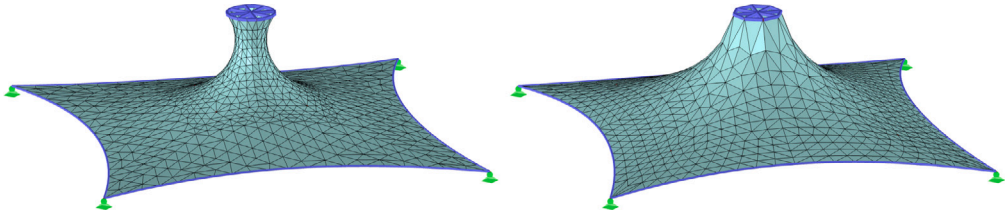

Fig. 17. Equilibrium shapes for the stress density method.

Regardless of the projection plane inclination selected, the above-mentioned independence between the final equilibrium state and the initial structure configuration resp. FE mesh discretization is valid in the stress projection procedure.

4.3. Shell structure

In the second example, form-finding analysis is used for the shape optimization of a shell structure to reach the membrane state of stresses under the applied self-weight. The compression forces specified for stress projection are defined as $\tilde{n}_{\bar{X}} = -10.00$ kN/m and $\tilde{n}_{\bar{Y}} = -5.00$ kN/m, or $\tilde{\mathbf{n}}_{\rho} = \{-10.00, -5.00, 0.00\}^T$ kN/m in vector form. For stress density and distortion control, the forces are $n_x = -10.00$ kN/m and $n_y = -5.00$ kN/m, or ${}^0\mathbf{n}_l = {}^l\mathbf{n}_l = \{-10.00, -5.00, 0.00\}^T$ kN/m in vector form. The base $\tilde{\mathbf{O}}$ coincides with the global coordinate system and, in fact, also with the local coordinate system of the surface in its initial position. Therefore, $\tilde{\mathbf{O}}$ coincides with the unit matrix $\tilde{\mathbf{O}} = \mathbf{I}$. In this case, the parameter $\lambda = 1.25$ can be higher compared to the previous example, as the shape does not tend to collapse or neck.

The initial planar configuration is shown in Fig. 18, consisting of two square shell surfaces with a side length of $l = 10.00$ m. Both shorter external sides of the shell structure are simply supported, and both longer sides are supported by two beams with the form-finding analysis requirement for a resulting length of $l_{be} = 11.22$ m. The four beams are simply supported in the middle of the longer sides and in the corners. The fifth beam is situated between the two square shells, with the form-finding requirement for a resulting length of $l_{bi} = 10.55$ m.

The equilibrium shapes are shown in Fig. 19, and the resulting state of the internal forces can be observed in Fig. 20.

The comparison of the resulting stress state is summarized in Table 3. It is again assumed that the ratio of the intended and the reached forces will be measured in terms of the resulting principal forces and the given input values, as the input values represent the initial principal

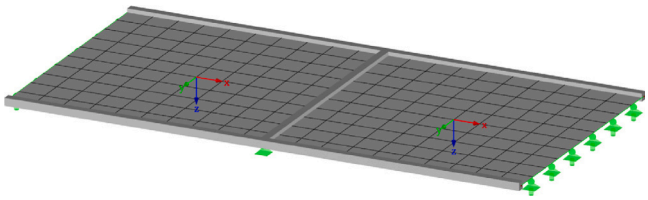

Fig. 18. Initial configurations of the shell structure.

forces. Moreover, the mesh quality in the equilibrium shape can be inspected and evaluated in terms of changes in element areas and angles between their sides. Therefore, the table also covers the results related to mesh quality.

In Table 3, a_k is the area of a particular finite element, while $\bar{a}$ and $|\Delta\bar{a}|$ represent the average element area within the structure and the average difference between the particular element size and this average value in an absolute value within the equilibrium position of the structure. Furthermore, $|\Delta\bar{\alpha}|$ represents the average angle deviation in an absolute value from the angle $\alpha = 90$ deg, measured between the two adjacent sides of the quadrangle elements. Lower values are better.

Compared with the previously performed form-finding analysis of the conical membrane structure, the differences recorded in Table 3 and Fig. 20 are not considerable. The most significant difference can be observed in the changes in finite element size. The essential reason for the lower in-plane movement of FE nodes when using stress projection lies in the orthogonality between the equilibrium within the horizontal projection plane and the vertical direction of gravitational acceleration, which is thus orthogonal to this projection plane. The stress projection does not require sliding the FE nodes in the in-plane direction of the shells to adapt the forces and reach the equilibrium, as is the case with the other methods. Interestingly, the only essential reason for the

Table 3
Comparison of the three stress adaptation procedures.

Evaluated quantities	Unit	Stress projection (SP)	Distortion control (DC)	Stress density (SD)
$\bar{n}_1$	kN/m	−4.84683	−4.61431	−3.79883
$\bar{n}_2$	kN/m	−10.39443	−10.91452	−13.37611
$\lvert\Delta\bar{n}_1\rvert = \frac{1}{m}\sum_{k=1}^{m} \lvert n_{1k} - \bar{n}_1\rvert$	kN/m	0.44862 (≈ 9.26%)	0.37445 (≈ 8.11%)	0.38444 (≈ 10.12%)
$\lvert\Delta\bar{n}_2\rvert = \frac{1}{m}\sum_{k=1}^{m} \lvert n_{2k} - \bar{n}_2\rvert$	kN/m	1.02505 (≈ 9.86%)	0.78366 (≈ 7.18%)	1.23595 (≈ 9.24%)
$\Delta n_1^* = \bar{n}_1 - (-5.00)$	kN/m	0.15317 (≈ −3.06%)	0.38569 (≈ −7.71%)	1.20117 (≈ −24.02%)
$\Delta n_2^* = \bar{n}_2 - (-10.00)$	kN/m	−0.39443 (≈ 3.94%)	−0.91452 (≈ 9.15%)	−3.37611 (≈ 33.76%)
$\bar{a}$	m²	0.8844	0.9007	0.9153
$\lvert\Delta\bar{a}\rvert = \frac{1}{m}\sum_{k=1}^{m} \lvert a_i - \bar{a}\rvert$	m²	0.0831 (≈ 9.40%)	0.2587 (≈ 28.72%)	0.1430 (≈ 15.62%)
$\lvert\Delta\bar{\alpha}\rvert = \frac{1}{4m}\sum_{k=1}^{m}(\sum_{j=1}^{4} \lvert\alpha_j - 90\rvert)_k$	deg	7.86978	7.04290	15.09133

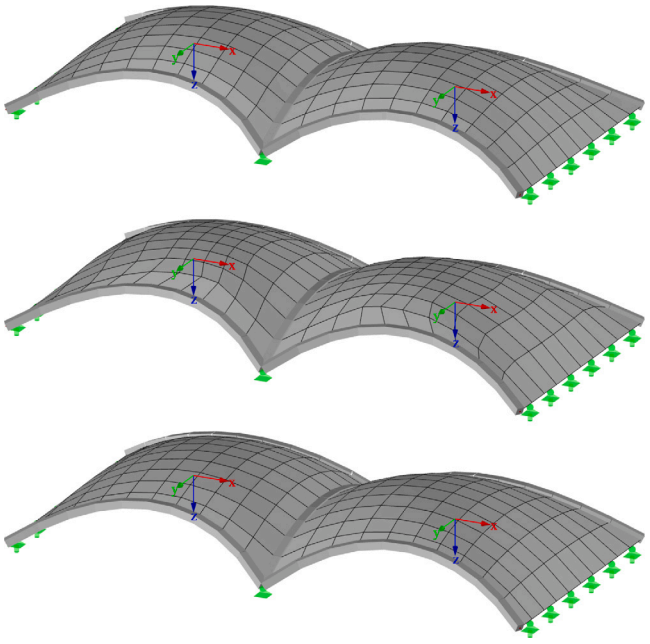

Fig. 19. Equilibrium shapes using stress projection (top), distortion control (middle), and stress density (bottom).

need to change the finite element sizes and shapes when using stress projection is to satisfy changes in the geometry itself between the initial and final equilibrium positions.

4.4. Complex membrane structure

The final example is a demonstrative complex membrane structure consisting of four conical parts and eight hyperbolic paraboloid parts. The conical membrane parts apply the proposed stress projection, while the hyperbolic parts apply the distortion control method. Generally, the proposed stress projection is especially suitable for the shape optimization of conical membrane and shell structures subjected to a permanent load. However, the stress projection is not intended for hyperbolic membrane structures or membranes on arches that are not susceptible to necking and collapsing during the form-finding analysis. In this case, the stress projection does not lead to a smoother distribution of prestress over the membrane structure compared to other stress adaptation schemes. For such shapes of membrane structures, other stress adaptation schemes can be utilized. Moreover, it is possible to combine different stress adaptation schemes without any problems when designing a complex structure, as shown in this last example. Such a combination allows structural engineers and architects to choose a suitable stress adaptation scheme for particular parts of a structure.

The example below presents a possible interaction between the proposed stress projection and other methods. The structural model of the membrane structure can be downloaded from the website of Dlubal Software in the section Downloads and Info, subsection Structural Analysis Models to Download, category Tensile Membrane Structures [33]. Here, the dimensions of the structure and the form-finding input and settings, as well as other details and information, can be found to verify the calculations. Interested readers are also encouraged to do their own evaluations by downloading the software [32], through which they can model any other structure, perform a form-finding analysis, and make the final evaluation.

In the following, the results of the form-finding analysis utilizing a combination of stress adaptation schemes are presented. A well-distributed prestress over the membrane structure can be observed in Figs. 21–23.

5. Discussion

Form-finding analysis deals with searching for the equilibrium shape of membrane and cable structures, and it can also be utilized for the shape optimization of shell and girder structures. However, the incompatibility between the analysis input, usually defined by two prestress values, and the difficulty of achieving the final double-curved surface shapes remains a challenge. Principally, the form-finding analysis needs to use a suitable stress adaptation scheme that is crucial for reaching the equilibrium, leading to the desirable final shape.

The proposed stress projection procedure is indeed a new stress adaptation scheme that allows for the calculation of equilibrium in space from the analytically predefined equilibrium in a selected projection plane. The stress state in the actual configuration is determined using a fictitious reference configuration obtained by the orthogonal projection. In a nutshell, the resulting shape is independent of the initial configuration or FE discretization of the structure. Numerical experiments demonstrate that the proposed stress projection can avoid undesirable stress concentrations in the flat areas of structures while leading to significant stress adaptations if the inclination is substantial. Considering the conical membrane structures, the stress concentrations are located near the hoop, where such a stress modification is inevitable. We believe that the proposed method can be utilized for the shape optimization of shell structures, which will be investigated in the near future.

Form-finding analysis is a delicate process, and there is no unique stress adaptation scheme that prevails over the others for general applications. The proposed stress projection has been proven to be powerful, especially for the form-finding analysis of conical membrane structures and the shape optimization of shell structures.

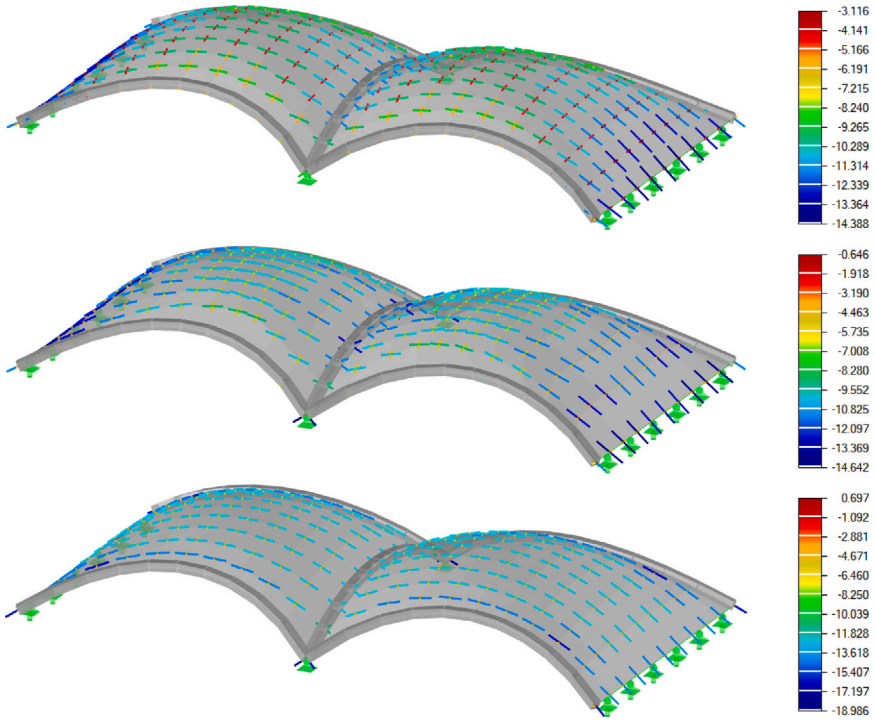

Fig. 20. Vectors of principal internal forces n_1 and n_2 [kN/m] using stress projection (top), distortion control (middle), and stress density (bottom).

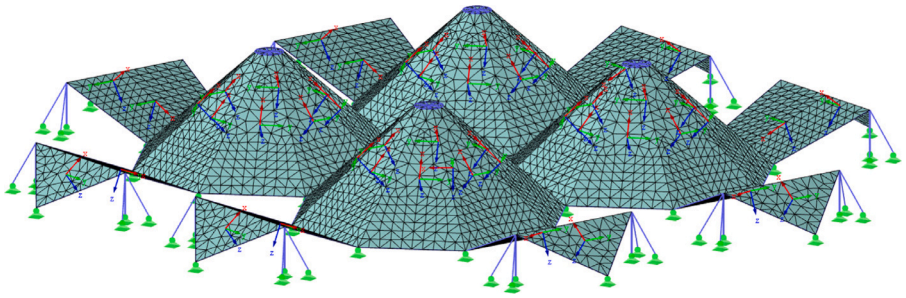

Fig. 21. Initial configurations of a complex membrane structure.

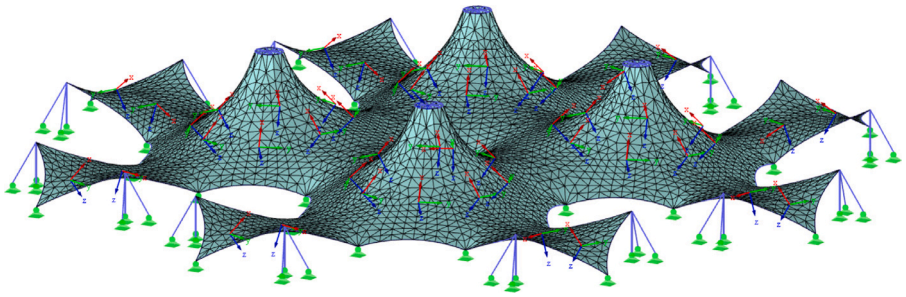

Fig. 22. Equilibrium shapes using a combination of stress projection and distortion control.

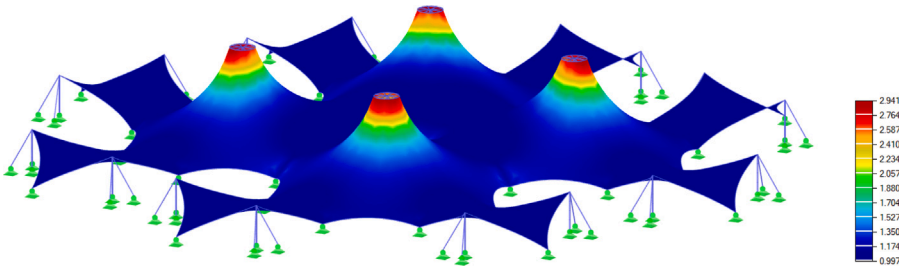

Fig. 23. First principal internal forces n_1 [kN/m].

CRediT authorship contribution statement

Ivan Němec: Supervision. **K.C. Park:** Writing – review & editing.

Declaration of competing interest

The authors declare that they have no known competing financial interests or personal relationships that could have appeared to influence the work reported in this paper.

Data availability

Data will be made available on request.

Acknowledgments

The research and development of this study were partially sponsored through the project Algorithmization of Form-finding of Membrane Structures and Its Static and Dynamic Analysis under project no. EG15_019/0004929, which was funded by the Ministry of Industry and Trade. International research cooperation was made possible through the project International Mobility of Researchers at Brno University of Technology II under project no. EF18_053/0016962, which was funded by the Ministry of Education, Youth, and Sports. The authors sincerely express their gratitude.

References

[1] Linhard J, Bletzinger KU. Tracing the equilibrium — Recent advances in numerical form finding. Int J Space Struct 2010;25(2):107–16. http://dx.doi.org/10.1260/0266-3511.25.2.107.

[2] Schek HJ. The force density method for form finding and computation of general networks. Comput Methods Appl Mech Engrg 1974;3(1):115–34. http://dx.doi.org/10.1016/0045-7825(74)90045-0.

[3] Linkwitz K, Schek H. Einige Bemerkungen zur Berechnung von vorgespannten Seilnetzkonstruktionen. Ing-Arch 1971;40(3):145–58. http://dx.doi.org/10.1007/bf00532146.

[4] Haber R, Abel J. Initial equilibrium solution methods for cable reinforced membranes part I—formulations. Comput Methods Appl Mech Engrg 1982;30(3):263–84. http://dx.doi.org/10.1016/0045-7825(82)90080-9.

[5] Maurin B, Motro R. The surface stress density method as a form-finding tool for tensile membranes. Eng Struct 1998;20(8):712–9. http://dx.doi.org/10.1016/S0141-0296(97)00108-9.

[6] Pauletti R, Pimenta P. The natural force density method for the shape finding of taut structures. Comput Methods Appl Mech Engrg 2008;197(49–50):4419–28. http://dx.doi.org/10.1016/j.cma.2008.05.017.

[7] Wüchner R, Bletzinger KU. Stress-adapted numerical form finding of pre-stressed surfaces by the updated reference strategy. Internat J Numer Methods Engrg 2005;64(2):143–66. http://dx.doi.org/10.1002/nme.1344.

[8] Bletzinger KU, Firl M, Linhard J, Wüchner R. Optimal shapes of mechanically motivated surfaces. Comput Methods Appl Mech Engrg 2010;199(5):324–33. http://dx.doi.org/10.1016/j.cma.2008.09.009.

[9] Bletzinger KU, Wüchner R, Daoud F. Equilibrium consistent anisotropic stress fields in membrane design. In: Textile composites and inflatable structures. Springer Netherlands; 2005, p. 143–51. http://dx.doi.org/10.1007/1-4020-3317-6_9.

[10] Bletzinger KU, Wüchner R. Form finding of anisotropic pre-stressed membrane structures. In: Trends in computational structural mechanics CIMNE. 2001.

[11] Haber R, Abel J. Initial equilibrium solution methods for cable reinforced membranes part II—implementation. Comput Methods Appl Mech Engrg 1982;30(3):285–306. http://dx.doi.org/10.1016/0045-7825(82)90081-0.

[12] Bletzinger KU, Ramm E. A general finite element approach to the form finding of tensile structures by the updated reference strategy. Int J Space Struct 1999;14(2):131–45. http://dx.doi.org/10.1260/0266351991494759.

[13] Bletzinger KU, Wüchner R, Daoud F, Camprubí N. Computational methods for form finding and optimization of shells and membranes. Comput Methods Appl Mech Engrg 2005;194(30):3438–52. http://dx.doi.org/10.1016/j.cma.2004.12.026.

[14] Tabarrok B, Qin Z. Nonlinear analysis of tension structures. Comput Struct 1992;45(5):973–84. http://dx.doi.org/10.1016/0045-7949(92)90056-6.

[15] Barnes M. Form-finding and analysis of prestressed nets and membranes. Comput Struct 1988;30(3):685–95. http://dx.doi.org/10.1016/0045-7949(88)90304-5.

[16] Barnes M. Form finding and analysis of tension structures by dynamic relaxation. Int J Space Struct 1999;14(2):89–104. http://dx.doi.org/10.1260/0266351991494722.

[17] Veenendaal D, Block P. An overview and comparison of structural form finding methods for general networks. Int J Solids Struct 2012;49(26):3741–53. http://dx.doi.org/10.1016/j.ijsolstr.2012.08.008.

[18] Tibert A, Pellegrino S. Review of form-finding methods for tensegrity structures. Int J Space Struct 2003;18(4):209–23. http://dx.doi.org/10.1260/026635103322987940.

[19] Lang R. Algorithms for design and analysis of membrane structures [Doctoral thesis], Brno: Brno University of Technology; 2019.

[20] Linkwitz K. Formfinding by the direct approach and pertinent strategies for the conceptual design of prestressed and hanging structures. Int J Space Struct 1999;14(2):73–87. http://dx.doi.org/10.1260/0266351991494713.

[21] Argyris J, Angelopoulos T, Bichat B. A general method for the shape finding of lightweight tension structures. Comput Methods Appl Mech Engrg 1974;3(1):135–49. http://dx.doi.org/10.1016/0045-7825(74)90046-2.

[22] Wood R. A simple technique for controlling element distortion in dynamic relaxation form-finding of tension membranes. Comput Struct 2002;80(27):2115–20. http://dx.doi.org/10.1016/S0045-7949(02)00274-2.

[23] Bletzinger KU, Ramm E. Structural optimization and form finding of light weight structures. Comput Struct 2001;79(22):2053–62. http://dx.doi.org/10.1016/S0045-7949(01)00052-9.

[24] Dutta S, Ghosh S. Form-finding of frame-supported tensile membrane structures using stochastic optimisation. Structures 2021;32:2211–21. http://dx.doi.org/10.1016/j.istruc.2021.03.103.

[25] Koohestani K. Nonlinear force density method for the form-finding of minimal surface membrane structures. Commun Nonlinear Sci Numer Simul 2014;19(6):2071–87. http://dx.doi.org/10.1016/j.cnsns.2013.10.023.

[26] Nguyen TN, Hien TD, Nguyen-Thoi T, Lee J. A unified adaptive approach for membrane structures: Form finding and large deflection isogeometric analysis. Comput Methods Appl Mech Engrg 2020;369:1–20. http://dx.doi.org/10.1016/j.cma.2020.113239.

[27] Shi JX, Wu Z, Tsukimoto S, Shimoda M. Design optimization of cable–membrane structures for form-finding and stiffness maximization. Compos Struct 2018;192:528–36. http://dx.doi.org/10.1016/j.compstruct.2018.03.033.

[28] Topping BHV, Ivanyi P. Computer aided design of cable membrane structures. In: Saxe-Coburg publications on computational engineering. Glasgow: Saxe-Coburg Publications; 2008.

[29] Marbaniang AL, Dutta S, Ghosh S. Updated weight method: An optimisation-based form-finding method of tensile membrane structures. Struct Multidiscip Optim 2022;65:1–22. http://dx.doi.org/10.1007/s00158-022-03262-5.

[30] Boudaoud A, Patricio P, Amar MB. The helicoid versus the catenoid: Geometrically induced bifurcations. Phys Rev Lett 1999;83(19):3836–9. http://dx.doi.org/10.1016/j.istruc.2021.03.103.

[31] FEM consulting – FEA calculation core development. 2022, Retrieved 30 September 2022, URL: https://www.fem.cz/.

[32] Dlubal software – Structural analysis and design software – Solutions – Analysis & design software for tensile membrane structures. 2022, Retrieved 30 September 2022, URL: https://www.dlubal.com/en/solutions/industries/analysis-and-design-software-for-tensile-membrane-structures.

[33] Dlubal software – structural analysis and design software – downloads and info – structural analysis models to download. 2022, Retrieved 30 September 2022, URL: https://www.dlubal.com/en/downloads-and-information/examples-and-tutorials/models-to-download.

[34] Dlubal software – structural analysis and design software – downloads and info – customer projects. 2022, Retrieved 30 September 2022, URL: https://www.dlubal.com/en/downloads-and-information/references/customer-projects.